THE RESPONSE OF A TWO-LAYER HYDROTHERMODYNAMIC OCEAN MODEL TO A SIMULATED MOVING HURRICANE

Stanley Holmes Grigsby

NAVAL POSTGRADUATE SCHOOL
Monterey, California

THESIS

THE RESPONSE OF A TWO-LAYER
HYDROTHERMODYNAMIC OCEAN MODEL
TO A SIMULATED MOVING HURRICANE

by

Stanley Holmes Grigsby

March 1975

Thesis Advisor: R. L. Elsberry

Approved for public release; distribution unlimited.

SECURITY CLASSIFICATION OF THIS PAGE (When Data Entered)

REPORT DOCUMENTATION PAGE		READ INSTRUCTIONS BEFORE COMPLETING FORM
1. REPORT NUMBER	2. GOVT ACCESSION NO.	3. RECIPIENT'S CATALOG NUMBER
4. TITLE (and Subtitle) The Response of a Two-Layer Hydrothermodynamic Ocean Model to a Simulated Moving Hurricane		5. TYPE OF REPORT & PERIOD COVERED Master's Thesis; March 1975 6. PERFORMING ORG. REPORT NUMBER
7. AUTHOR(s) Stanley Holmes Grigsby		8. CONTRACT OR GRANT NUMBER(s)
9. PERFORMING ORGANIZATION NAME AND ADDRESS Naval Postgraduate School Monterey, California 93940		10. PROGRAM ELEMENT, PROJECT, TASK AREA & WORK UNIT NUMBERS
11. CONTROLLING OFFICE NAME AND ADDRESS Naval Postgraduate School Monterey, California 93940		12. REPORT DATE March 1975 13. NUMBER OF PAGES 68
14. MONITORING AGENCY NAME & ADDRESS(if different from Controlling Office) Naval Postgraduate School Monterey, California 93940		15. SECURITY CLASS. (of this report) Unclassified 15a. DECLASSIFICATION/DOWNGRADING SCHEDULE

16. DISTRIBUTION STATEMENT (of this Report)

Approved for public release; distribution unlimited.

17. DISTRIBUTION STATEMENT (of the abstract entered in Block 20, if different from Report)

18. SUPPLEMENTARY NOTES

19. KEY WORDS (Continue on reverse side if necessary and identify by block number)

Air-Sea Interaction
Hurricane Model
Ocean Model
Convective Mixing
Wind Mixing
Advection
Hydrothermodynamic
Upwelling
Inertial Flow

20. ABSTRACT (Continue on reverse side if necessary and identify by block number)

The time dependent mixed-layer depth and temperature response of a two-layer hydrothermodynamic ocean model to a moving hurricane model was investigated. The hurricane model was that of Elsberry, Pearson, and Corgnati (1974). The maximum eye radius and hurricane intensity was bounded to isolate ocean reaction from hurricane variance. The ocean model was based on the upwelling model of O'Brien and

DD FORM 1 JAN 73 1473 EDITION OF 1 NOV 65 IS OBSOLETE
S/N 0102-014-6601 |
(Page 1)

SECURITY CLASSIFICATION OF THIS PAGE (When Data Entered)

Block 20 - ABSTRACT (Cont.)

Hurlburt (1972) in two dimensions and was located along the path of the storm. The momentum and depth equations in this model are treated semi-implicitly. Mechanical and convective mixing was included and was found to be the dominate cause of deepening of the mixed layer and cooling of the ocean surface. Alternating regions of upwelling and downwelling were produced in the wake of the storm as a result of inertial waves caused by the passage of the storm. The cases studied indicated a linear relation between the wavelength and the storm translation speed.

The Response of a Two-Layer Hydrothermodynamic Ocean Model to a Simulated Moving Hurricane

by

Stanley Holmes Grigsby
Lieutenant, United States Navy
B.S., Kansas State College of Pittsburg, 1968

Submitted in Partial Fulfillment of the
requirements for the degree of

MASTER OF SCIENCE IN METEOROLOGY

from the

NAVAL POSTGRADUATE SCHOOL
March 1975

ABSTRACT

The time dependent mixed-layer depth and temperature response of a two-layer hydrothermodynamic ocean model to a moving hurricane model was investigated. The hurricane model was that of Elsberry, Pearson, and Corgnati (1974). The maximum eye radius and hurricane intensity was bounded to isolate ocean reaction from hurricane variance. The ocean model was based on the upwelling model of O'Brien and Hurlburt (1972) in two dimensions and was located along the path of the storm. The momentum and depth equations in this model are treated semi-implicitly. Mechanical and convective mixing was included and was found to be the dominate cause of deepening of the mixed layer and cooling of the ocean surface. Alternating regions of upwelling and downwelling were produced in the wake of the storm as a result of inertial waves caused by the passage of the storm. The cases studied indicated a linear relation between the wavelength and the storm translation speed.

TABLE OF CONTENTS

LIST OF TABLES

LIST OF FIGURES

TABLE OF SYMBOLS

A	diffusion constant = $10^2 m^2/sec$
c	drag coefficient at the interface = 3×10^{-4}
c_p	specific heat of water = 4179. joules/Kg Kelvin
D	dissipation of energy
f	coriolis parameter = 6.16176×10^{-5} sec^{-1}
G	kinetic energy from the wind
g	gravitational acceleration = 9.8 m/sec^2
g'	$g(\rho_2-\rho_1)/\rho_2$ = .02 m/sec^2
H_1	representative thickness of upper layer ≡ 30 meters
H_2	representative thickness of lower layer ≡ 100 meters
h_1	thickness of the upper layer
h_2	thickness of the lower layer
h_1'	$h_1 - H_1$
h_2'	$h_2 - H_2$
Q_E	heat flux at the surface due to evaporation
Q_S	sensible heat flux at the surface
T_h	temperature at the top of the thermocline
$T_1=T_S$	temperature of the upper layer
T_2	average temperature of the thermocline
u_1	depth averaged radial component of current in the upper layer
u_2	depth averaged radial component of current in the lower layer
v_1	depth averaged tangential component of current in the upper layer
v_2	depth averaged tangential component of current in the lower layer

w_1	vertical motion at the interface of the two layers
Λ	entrainment function
ρ	density of water = 1024 kg/m
τ^{B_x}	x-component of the stress at the bottom of the lower layer
τ^{B_y}	y-component of the stress at the bottom of the lower layer
τ^{I_x}	x-component of the stress at the interface
τ^{I_y}	y-component of the stress at the interface
τ^{S_x}	x-component of the surface stress
τ^{S_y}	y-component of the surface stress

ACKNOWLEDGEMENT

The author wishes to express his appreciation to Dr. R.L. Elsberry for his time, patience, and guidance and to Dr. D.F. Leipper and Dr. R.L. Haney for their constructive comments.

The author also offers his gratitude to the personnel of the W.R. Church Computer Center, especially Mr. W.D. Ehrman, consultant, for aid in the development of the output package of the program.

Last, but not least, the author wishes to express his gratitude to his wife, Donna, for her understanding and her typing, and to his daughters, Kimberly and Michelle, for their patience during this study.

I. INTRODUCTION

It is generally accepted that sea-surface temperatures may be strongly affected by tropical storm activity, and vice versa. Sea-surface temperatures in excess of 26°C are apparently required to produce hurricane-force winds. It has also been observed that cooling of as much as 6°C may be present in the wake of a hurricane.

One of the first systematic efforts to investigate the cooling effect was done after the passage of hurricane Hilda, 1964. From this data, Leipper (1967) found clear evidence supporting previous scattered observations which indicated lowering of sea-surface temperatures in the wake of a hurricane. The sea-surface temperature was observed to drop 5 to 6°C from the temperature present before the storm passage. The observations indicated upwelling from about 60 m in depth. Associated with this was an outward transport of water which occurred in the warm surface layers with cooling and mixing of these layers as they moved outward. Finally this outward moving water experienced convergence and downwelling around the hurricane area. The observations were taken along paths perpendicular to the path followed by the storm. This would not allow certain features along the path of the storm to be observed, for example, the internal waves predicted by Geisler (1970).

In conjunction with project Stormfury, Black and Mallinger (1972) reported on data taken before, during, and after the passage of hurricane Ginger, 1971. These oceanic measurements were taken from a Navy WP-3 aircraft using airborne expendable bathythermographs, (AXBTs). The primary information gained, of interest in this thesis, was that as the storm moved faster less surface cooling occurred. In fact, there appeared to be a cut-off speed related to the ratio of the baroclinic wave speed and the speed of propagation of the storm. Geisler (1970) predicted this ratio to be $\sqrt{2}$ whereas the data obtained suggested a ratio of 3. At the slower speeds strong upwelling near the center should occur. While, at the faster speeds the upwelling intensity decreases, and therefore does not contribute greatly to the surface cooling.

Sheets (1974) presented evidence indicating internal gravity waves at the thermocline in the wake of a rapidly moving hurricane, Ellen, 1973. A total of 18 AXBTs were dropped at intervals of five to fifteen nautical miles. In addition to the internal wave indication, a surface cooling of .5°C to 1.5°C was observed. The amount of surface cooling is in agreement with the concept that a rapidly moving storm does not cool the ocean surface to the same extent as slower moving storms. In the same paper, however, data from hurricane Irah, a slow moving storm (7-10 kt), showed nominal cooling, less than .5°C, instead of the greater anticipated cooling. These data illustrate that many factors play

a part in the response of the ocean surface temperature to the passage of a hurricane.

O'Brien and Reid (1967) developed a model of the time-dependent response of a two-layer (one active layer) ocean model under a stationary, axially-symmetric atmospheric vortex. The dynamic response of the ocean was also assumed to be axially-symmetric, and therefore solutions in two independent variables, radial distance and time, could be obtained. Gradient winds were obtained from a pressure distribution function resembling actual data. The surface stress was derived using these winds. The results of this model indicated strong upwelling near the center due to velocity divergence. This upwelling was strongest near the region of maximum surface stress. After 48 hours the depth of the upper layer had been reduced to about 10 meters in the region of maximum upwelling.

Geisler (1970) developed a model of the linear response of a two-layer ocean to a stress pattern representing a hurricane moving at a constant speed. When the speed of movement was greater than the baroclinic wave speed, this model produced internal waves at the interface of the mixed layer and the thermocline in the wake of the storm. The wavelength of these disturbances increased as the speed of movement of the storm increased. The disturbance propagated in the same direction and at the same speed as the storm. Another feature of this model was that a baroclinic ridge was left in the ocean in the wake of the storm. Due to

upwelling near the center and downwelling in the surrounding area, a wake of reduced mixed-layer depth near the center of the path was produced. The amplitude of this ridge was greater with decreasing speed of movement of the hurricane.

The models discussed thus far treated only the response of the ocean to a given wind stress. In an effort to develop a model to describe the interaction of the ocean and the atmosphere during a hurricane, Elsberry, Pearson and Corgnati (1974) developed an axisymmetric hurricane model. As the atmospheric portion of this model is used in this thesis it will be described later. The ocean used in this case was at a fixed temperature.

Fraim (1973) introduced a mixed-layer model capable of producing time-dependent values of sea-surface temperature and mixed-layer depth in response to atmospheric forcing. It was based on the mixed-layer models of Kraus and Turner (1967), and Denman (1973), which predicted the mixed-layer temperature and depth in response to wind mixing and convection. The radial current was defined by the Ekman current response to the stress at the surface. In this model the stress input to wind mixing, τ_0, was a function of the total stress, τ_a, the roughness length, Z_0, the mixed-layer depth, h_0, and an adjustable constant C.

$$\tau_0 = \tau_a \, \mathrm{EXP}(- \frac{h_0}{CZ_0})$$

The excess stress, $\tau_a - \tau_0$, was used to produce currents from Ekman balance considerations. This yielded a depth-averaged

radial current, and due to symmetry, this is the only current which could produce upwelling. Application of the continuity equation to these values of current gave the upwelling at the bottom of the mixed layer. This model was used to study the effects of the three cooling processes involved in lowering the sea surface temperatures. These are, entrainment mixing across a stable layer, convective mixing, and vertical and horizontal advection. The results of these experiments showed that both advection and mixing have significant effects on the sea surface temperature and mixed layer depths, and as expected these effects are most pronounced in the region of maximum surface stress.

Trapnell (1974) introduced more refinements into the Fraim model, the most notable of which was the addition of a return flow in the lower layer and the ability to let the surface stress move across the ocean. The flow in the lower layer was assumed to have the same mass transport as the upper layer. This added a new method by which the below layer gradient could be changed. In addition to upwelling and downwelling, there now existed horizontal advection. Movement of the stress and cooling functions was simulated by translating the center of the atmosphere grid relative to the ocean grid. This adjustment was made at certain time increments to simulate different speeds. The results from Trapnell's experiments suggest that entrainment mixing is the primary mechanisms for cooling the oceans, except within the region of maximum winds where intense upwelling becomes

important. Also it is seen that these effects are strongly associated with slower moving storms. Due to the lack of dynamics this model did not exhibit the internal waves predicted by Geisler.

One of the primary constraints in both Fraim's and Trapnell's models was that the currents used were derived from Ekman balance to a given surface stress. As a further refinement, this thesis describes a two-layer hydrothermodynamic model and its response to surface stress and cooling representing a moving hurricane.

II. MODEL

A. OCEAN MODEL

The dynamical equations in the ocean model and the method of solution described in this thesis follow the coastal upwelling model of O'Brien and Hurlburt (1972). However the present model contains a term to include thermal and mechanical mixing due to upward heat flux and mechanical energy input at the surface.

$$\frac{\partial u_1}{\partial t} + u_1\frac{\partial u_1}{\partial x} + g\frac{\partial}{\partial x}(h_1+h_2) = fv_1 + \frac{\tau^{S_x}_{-\tau^{I_x}}}{\rho h_1} + A\frac{\partial^2 u_1}{\partial x^2} \qquad (1)$$

$$\frac{\partial u_2}{\partial t} + u_2\frac{\partial u_2}{\partial x} + g\frac{\partial}{\partial x}(h_1+h_2) - g'\frac{\partial h_1}{\partial x} = fv_2 + \frac{\tau^{I_x}_{-\tau^{B_x}}}{\rho h_2} + A\frac{\partial^2 u_2}{\partial x^2} \qquad (2)$$

Equations (1) and (2) are the radial momentum equations in the upper and lower layers respectively. These include the advection, pressure gradient, coriolis, stress, and lateral diffusion terms.

$$\frac{\partial v_1}{\partial t} + u_1\frac{\partial v_1}{\partial x} = -fu_1 + \frac{\tau^{S_y}_{-\tau^{I_y}}}{\rho h_1} + A\frac{\partial^2 v_1}{\partial x^2} \qquad (3)$$

$$\frac{\partial v_2}{\partial t} + u_2\frac{\partial v_2}{\partial x} = -fu_2 + \frac{\tau^{I_y}_{-\tau^{B_y}}}{\rho h_2} + A\frac{\partial^2 v_2}{\partial x^2} \qquad (4)$$

These are the tangential momentum equations, comprised of the same terms as the radial momentum equations, excepting the pressure gradient forces, which due to symmetry are zero.

The stress in the momentum equations is defined by

$$\tau^{S_x} = -k\,\tau_a \sin\alpha \tag{5a}$$

$$\tau^{S_y} = k\,\tau_a \cos\alpha \tag{5b}$$

where k is the partitioning constant which determines how much of the surface stress will be used for current generation, and α is the atmospheric inflow angle. Following O'Brien and Hurlburt (1972) the stress components of the interface are defined as

$$\tau^{I_x} = \rho_w c\bar{q}(u_1-u_2) \tag{6a}$$

$$\tau^{I_y} = \rho_w c\bar{q}(v_1-v_2) \tag{6b}$$

where $\bar{q} = (q_1+q_2)/2$

and $q_i = (u_i^2+v_i^2)^{\frac{1}{2}}$

The constant c is the drag coefficient at the interface, and is chosen to be 3×10^{-4} also following O'Brien and Hurlburt.

$$\frac{\partial h_1}{\partial t} + \frac{\partial h_1 u_1}{\partial x} = \frac{1}{T_s-T_h}\left[\frac{2}{h_1}(G-D) + \frac{Q_E+Q_S}{\rho c_p}\right] \equiv M \tag{7}$$

$$\frac{\partial T_1}{\partial t} + \frac{\partial T_1 u_1}{\partial x} - \frac{w_1 T_s}{h_1} + \frac{\Lambda M}{h_1}(T_s-T_h) - \frac{Q_E+Q_S}{\rho c_p h_1} = 0 \tag{8}$$

Equations (7) and (8), which describe the temperature and depth of the mixed layer, are the same as used by Fraim (1973) and Trapnell (1974). The term M is the contribution to depth change due to entrainment mixing. The increase in potential energy of the column through entrainment at the interface is equal to the excess of mechanical generation (G) of kinetic energy over dissipation (D), plus a contribution due to convective overturning if the column is losing heat ($Q_E+Q_S > 0$). Λ is called the entrainment parameter which is 1 when M is positive and zero when M is negative. Thus mixing across the base of the mixed layer occurs only when M is positive, and therefore acting to deepen and cool the mixed layer. If M were permitted to be negative it would simulate heat extraction from the lower layer, to warm the already warmer upper layer. As this model depicts a wind dominated region, M is always 1.

$$\frac{\partial h_2}{\partial t} + \frac{\partial h_2 u_2}{\partial x} = -M \qquad (9)$$

$$\frac{\partial T_2}{\partial t} + \frac{\partial T_2 u_2}{\partial x} + \frac{w_1 T_h}{h_2} = 0 \qquad (10)$$

Equations (9) and (10) are the equivalent equations to (3) and (4) but in the lower layer. Mixing does not contribute directly to the change in temperature at that level, therefore only the advection and vertical motion terms are present. It can be shown that with the assumed linear distribution of currents and temperatures in the lower layer,

that the temperature advected by the average current component is that from a level 2/3 of the distance from the bottom of the lower layer.

$$w_1 = -h_2 \frac{\partial u_2}{\partial x} \tag{11}$$

$$T_h = 2T_2 - T_b \tag{12}$$

Equations (11) and (12) are diagnostic equations used to close the equation set. Equation (11) was derived by integrating the continuity equation in the lower layer and using the boundary conditions of no mass flux through the bottom of that layer. Equation (12) utilizes the fixed bottom temperature, the linear lapse rate assumption, and the newly computed values of the depth and average temperature of the lower layer to compute a new value of temperature at the top of the thermocline, T_h.

The boundary conditions allowed no heat or momentum flux through the ends or bottom of the model. At the surface a momentum flux from the atmosphere to the ocean was applied. A heat flux from the ocean to the atmosphere also occurred at the surface. The model was considered to be a free surface model because the height of the ocean surface varied with respect to the fixed bottom depth.

As in O'Brien and Hurlburt the solutions to the equations contain external and internal gravity waves. Therefore the pressure gradient terms in the radial momentum equations were treated implicitly to allow a longer time

step to be taken and still retain these waves. Treatment of these equations is shown in Appendix A. The remainder of the equations were evaluated using centered differencing in time and space. Stability problems will occur due to using centered differences in both time and space in the diffusion term, therefore time lag was used in this term.

The atmospheric parameters were computed at 100 grid points with a three kilometer spacing. This atmospheric forcing was moved at a constant speed across this grid in order to simulate the motion of a storm. The atmospheric forcing was applied to the ocean model as shown in figure 1. Between and including C and D the atmospheric forcing parameters were applied directly, from D to E the values at D were applied. The values from C to D in the atmosphere were applied to the points from C to B in the ocean, although the sign was changed on the stress terms for symmetry. From point B to point A the values at point B were applied. Points B, C, and D move from right to left to simulate the motion of the storm.

As in Trapnell's model the surface stress and heating functions were not initially applied at full value. To permit the initially quiet ocean to adjust, the forcing was increased exponentially, requiring about nine hours for application of 95% of the full force of the storm. It was found that both the atmospheric and oceanic models remained stable for time steps of 900 seconds.

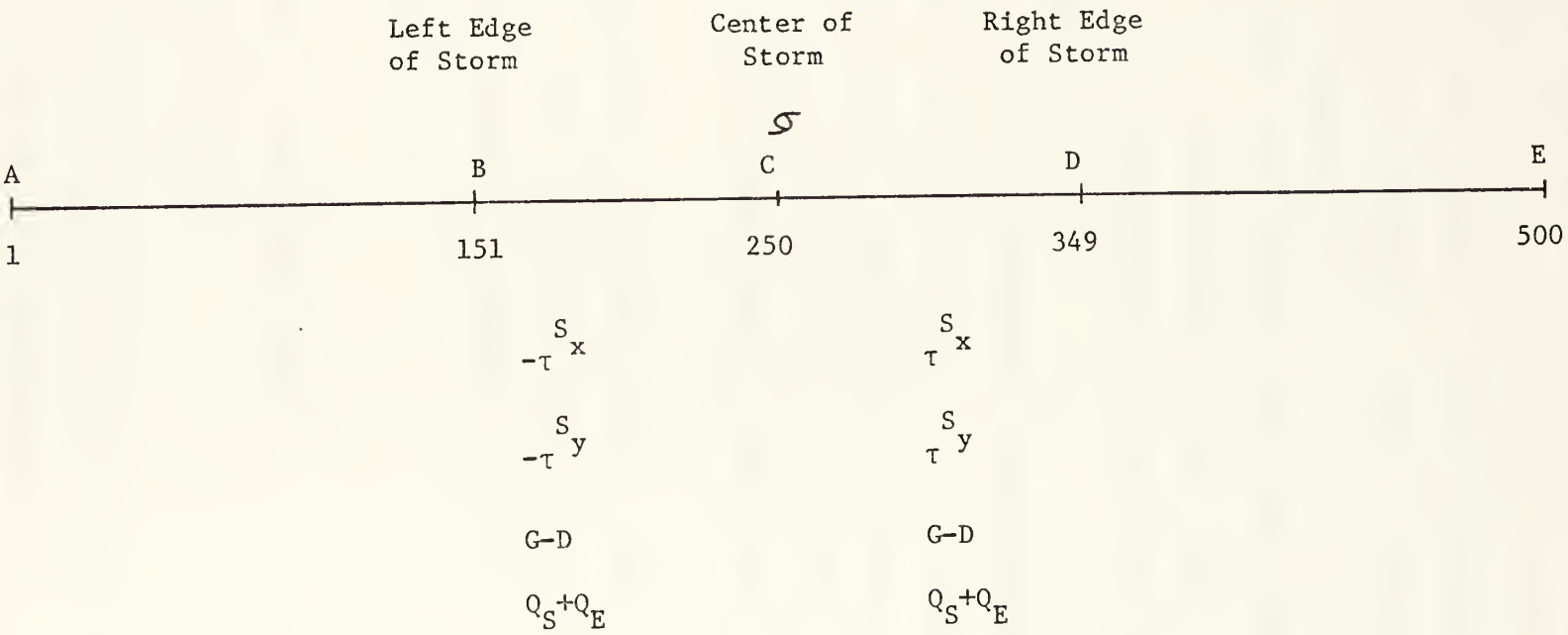

Figure 1. Schematic of the Storm Moving Along the Grid.

B. ATMOSPHERIC MODEL

The atmospheric hurricane model used to drive the ocean in these experiments is the two-layer, time-dependent model of Elsberry, Pearson, and Corgnati (1974) which was also used in the moving model by Trapnell (1974). The hurricane was considered to be mature so that an axially-symmetric storm could be assumed. The maximum winds were permitted to intensify to 50 m sec^{-1} and then held fixed. This allowed the changes in the ocean structure to be isolated from changes in the atmospheric model.

The atmospheric model was integrated simultaneously during these experiments using the new sea-surface temperatures computed by the ocean model. New surface stresses and surface heating values were also applied to the ocean. This constituted the interaction between the ocean and the atmosphere.

This model consisted of a surface inflow layer and an upper outflow layer. The tangential wind flow at the surface outside the radius of maximum winds was given by

$$V_\theta r^{\frac{1}{2}} = \text{const}$$

and inside the radius of maximum winds by

$$V_\theta r^{-1} = \text{const.}$$

These equations were empirically derived by Riehl (1963) and supported by observations by Gray and Shea (1973). The radius of maximum wind was assumed to coincide with the

eyewall radius. Normally in this model the eyewall radius is defined to be that radius at which the average of five adjacent values of equivalent potential temperature was a maximum. However, to isolate the changes in the ocean, the eyewall radius was fixed at 30 km after a short period of adjustment. The boundary layer in the atmospheric model was a two-layer, baroclinic model developed by Cardone (1969). The heat and momentum fluxes at the interface were computed in this model. These were a function of the stability of the boundary layer and the wind at the top of this layer. To obtain more information regarding the atmospheric model the paper by Elsberry, Pearson, and Corgnati (1974) should be consulted.

III. RESULTS

A. EFFECTS OF TRANSLATION SPEED

The simulated storm was moved at various speeds, and compared with the stationary case to observe the changes in the behavior of the ocean due to storm translation speed. Many of the model results are consistent with previous theories and observations, as discussed earlier. The behavior of selected ocean parameters is displayed in figures 3 through 6 and 10 through 13. The parameters displayed in these figures are:

a) the temperature at the top of the thermocline;

b) the temperature of the mixed layer, and therefore the ocean surface:

c) the depth of the mixed layer;

d) the vertical velocity as derived from the continuity equation in the lower layer;

e) the upper-level current component directed along the path of the storm (positive values indicate a current toward the right; also note that the baseline is at $-.1$ m sec^{-1});

f) the tangential wind velocity at the top of the atmospheric boundary layer (the stress outside the storm is held at the value present at the outer edge of the storm, rather than being zero as implied by this graph).

In the standard model half of the surface stress was used to produce currents, and half was used for energy input to entrainment mixing. The total surface stress had a maximum value of 2.6 nt m^{-2} (26 dynes cm^{-2}). The mixed layer had an initial depth of 30 m and temperature of 30°C, while the lower layer, the thermocline, extended 100 m below the mixed layer and terminated with a fixed bottom temperature of 20°C. This initial state is depicted in figure 2. As can be seen from figure 2, a small ledge in the temperature appears at the bottom of the mixed layer. From Eq. (7) it is seen that if T_s is equal to T_h the term M becomes infinite. To maintain a slightly stable layer at the interface, this difference is initialized at .1 degree and never allowed to become smaller in magnitude. However, as this temperature difference immediately increases in response to the wind mixing, the condition was not forced following initialization.

1. Stationary Storm Model

The results after integration for 36 hours with the translation speed equal to zero are displayed in figure 3. The wind profile is shown in figure 3f. Note that this does not depict the wind outside the storm area. The vertical motion at the bottom of the mixed layer is displayed in figure 3d. Combining this with the radial currents in the upper layer, as shown in figure 3e, we see there are two circulation cells on each side of the storm center. The first cell has its maximum upwelling at the inside edge of

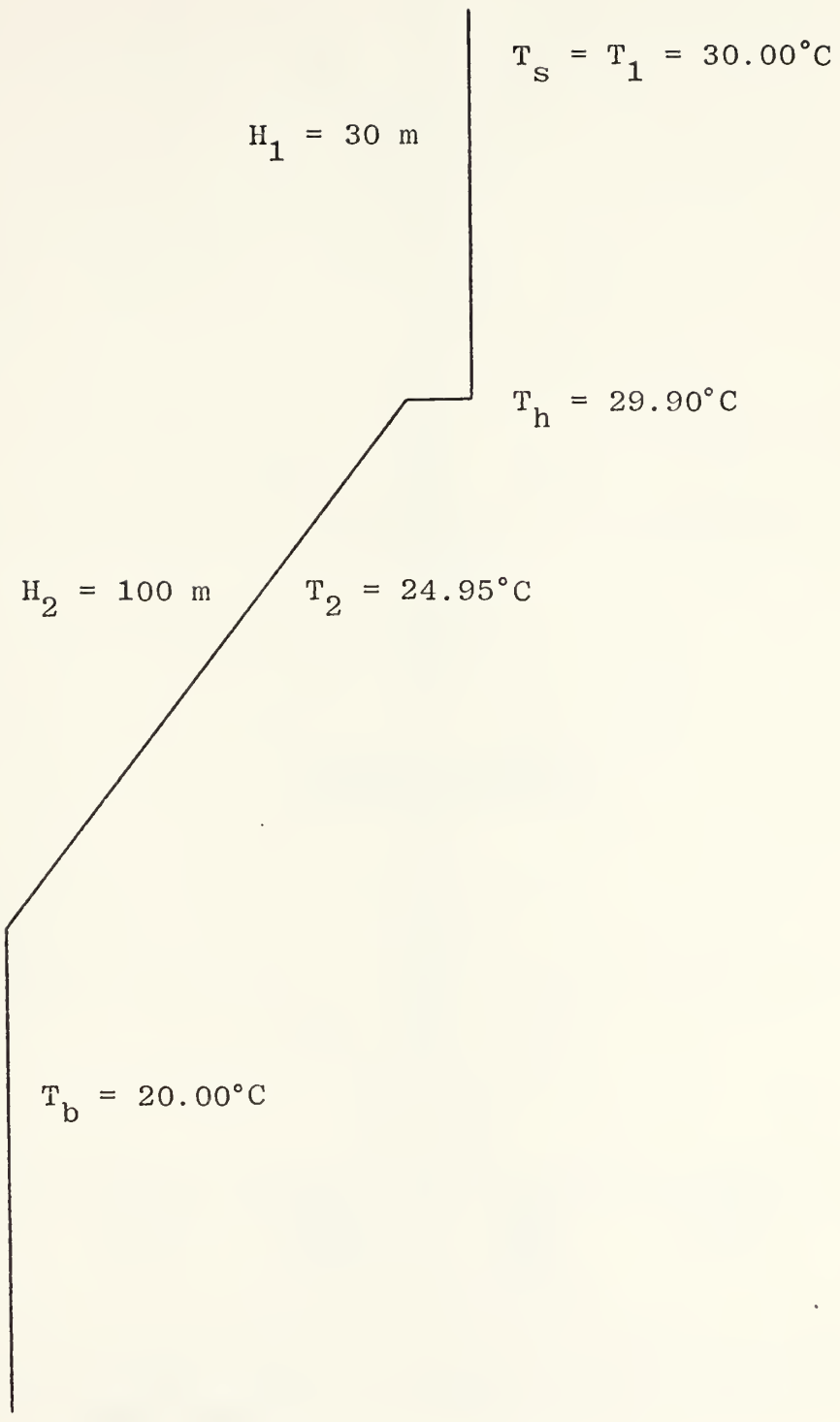

Figure 2. Initial Ocean Structure

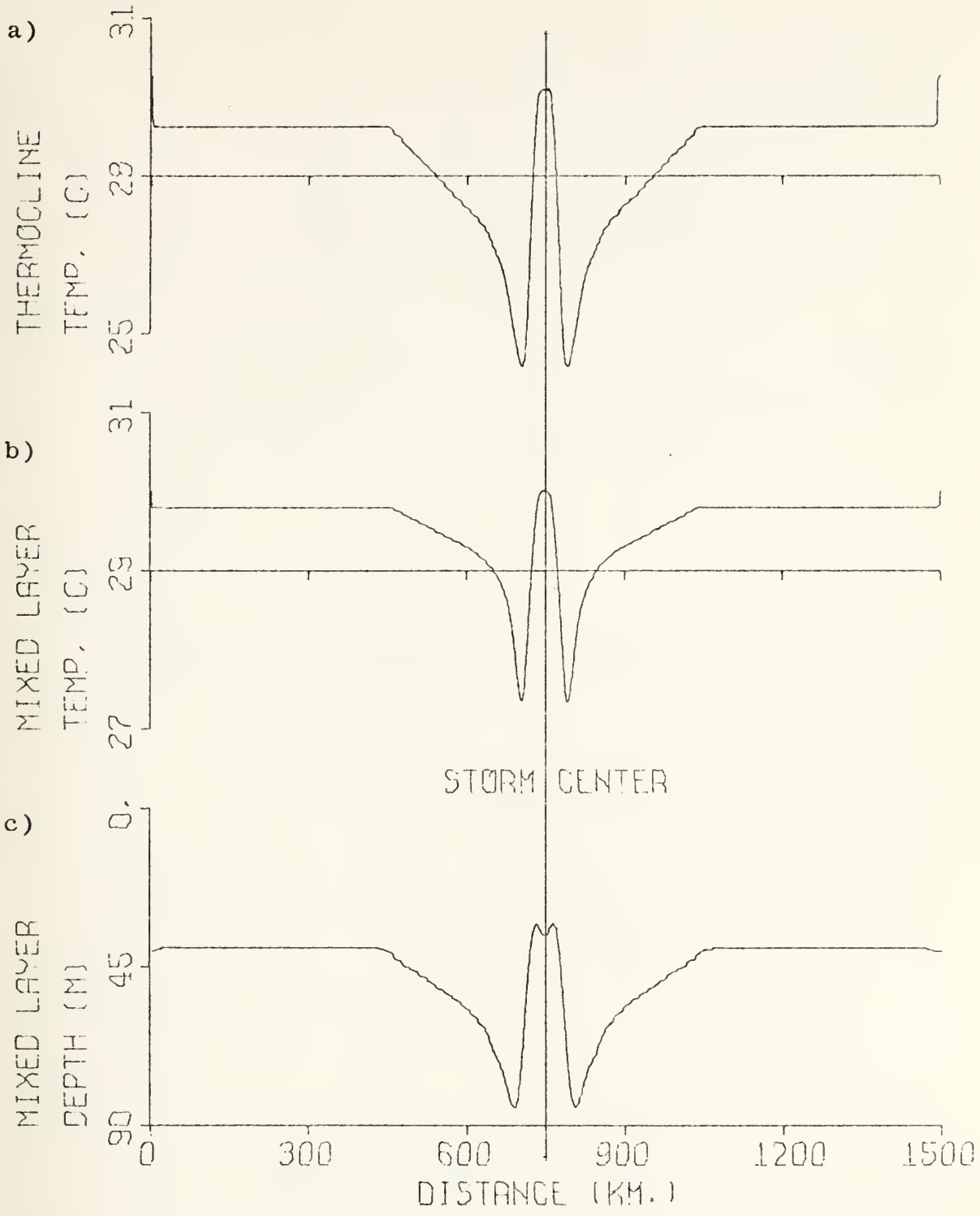

Figure 3. 36 Hour Predicted Values for the Stationary Storm Case.

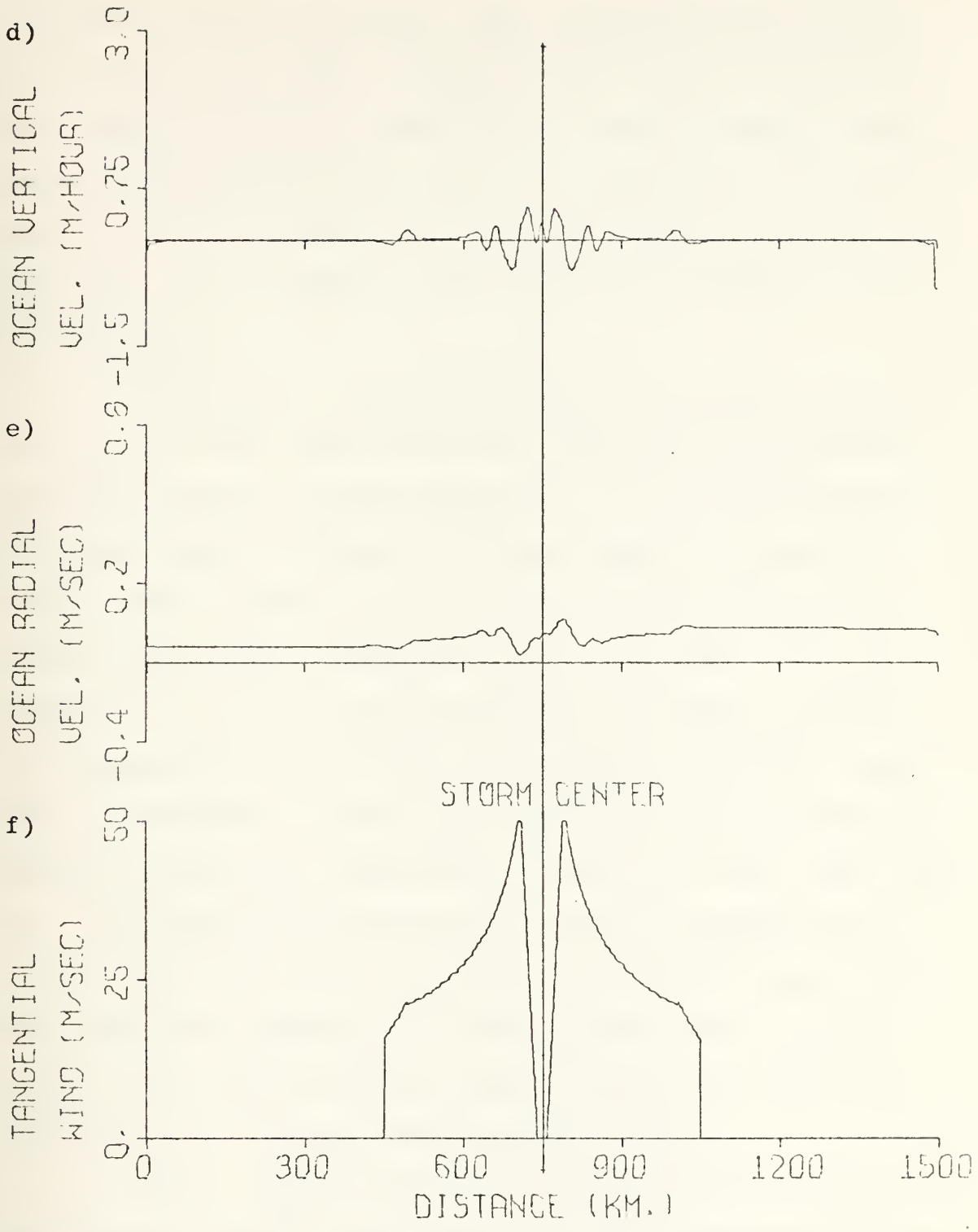

Figure 3. (Cont.) 36 Hour Predicted Values for the Stationary Storm Case.

the radius of maximum winds, RMW, and downwelling at the outer edge of the RMW. A second cell of about half the magnitude is located at about 90 km from the center. The maximum depth of the mixed layer is observed at the outer edge of the RMW, rather than coincident with it as might be expected. At the RMW the deepening due to mixing is offset by upwelling.

Referring to figures 3b and 3d the minimum temperature of the mixed layer does not correspond to the maximum upwelling region, or from figure 3c, to the maximum depth of the mixed layer. Instead the lowest temperatures are directly under the RMW, indicating that both upwelling and mixing contribute to cooling of the upper layer. The temperature at the top of the thermocline is shown in figure 3a. Deepening of the mixed layer, and the resultant reduction in thickness of the lower layer, would be the greatest factor in the lower temperature at the top of the lower layer. The reduced thickness would lower the temperature directly due to the lower position on the thermal lapse rate. The water being advected into this region would also be colder, thus contributing to lower temperatures (see the discussion of T_2 in the model equation (10)).

Table I compares Trapnell's Ekman current model with this dynamic model. The results are for a stationary storm case after being integrated 18 hours. The major difference is in the minimum mixed layer depth. This could be due to the slower reaction of the dynamic model, as this value was

TABLE I

Comparison of Stationary Storm Cases of Trapnell's Ekman Currents Model and the Dynamic Model, After 18 Hours

	Ekman	Dynamic
Maximum upper level radial current	.28 m/sec^{-1}	.31 m/sec^{-1}
Maximum downwelling	.48 m/hr^{-1}	.54 m/hr^{-1}
Maximum upwelling	1.18 m/hr^{-1}	1.66 m/hr^{-1}
Minimum mixed layer depth	17.2 m	34.6 m
Maximum mixed layer depth	72.6 m	65.2 m
Minimum mixed layer temperature	28.85°C	28.5 °C
Maximum mixed layer temperature	30.09°C	30.0 °C

about 24 m after 27 hours. Another explanation could be the different method of partitioning the surface stress. From this comparison the results from a model using currents in Ekman balance appear to compare favorably with the dynamic model.

2. Moving Storm Model

The results of moving the storm at 3.2 kt for 72 hours are shown in figure 4. Comparing figure 4b with figure 3b, it is seen that a minimum mixed-layer temperature of 28.3°C was observed as compared to 27.3°C associated with the stationary storm. Evidence of waves on the interface at the bottom of the mixed layer is shown in figure 4c. The wavelength is about 180 km. These waves are more noticeable in the vertical and upper layer radial velocities in figures 4d and 4e.

The comparison of Trapnell's Ekman model moving at 3.39 kt and the dynamic model moving at 3.2 kt is shown in Table II. The main difference is the momentum terms, however overall these values of maximums and minimums do not differ greatly. The problem with the Ekman model is that it does not contain the dynamics necessary to produce the horizontal distribution of variables that are present in figure 4. It appears that for sea-surface temperature prediction the Ekman balance model would produce comparable results to the more complicated dynamic model. However for a prediction of the internal structure of the ocean, (e.g. mixed-layer depth, slope of the thermocline, etc.) the dynamic model is necessary.

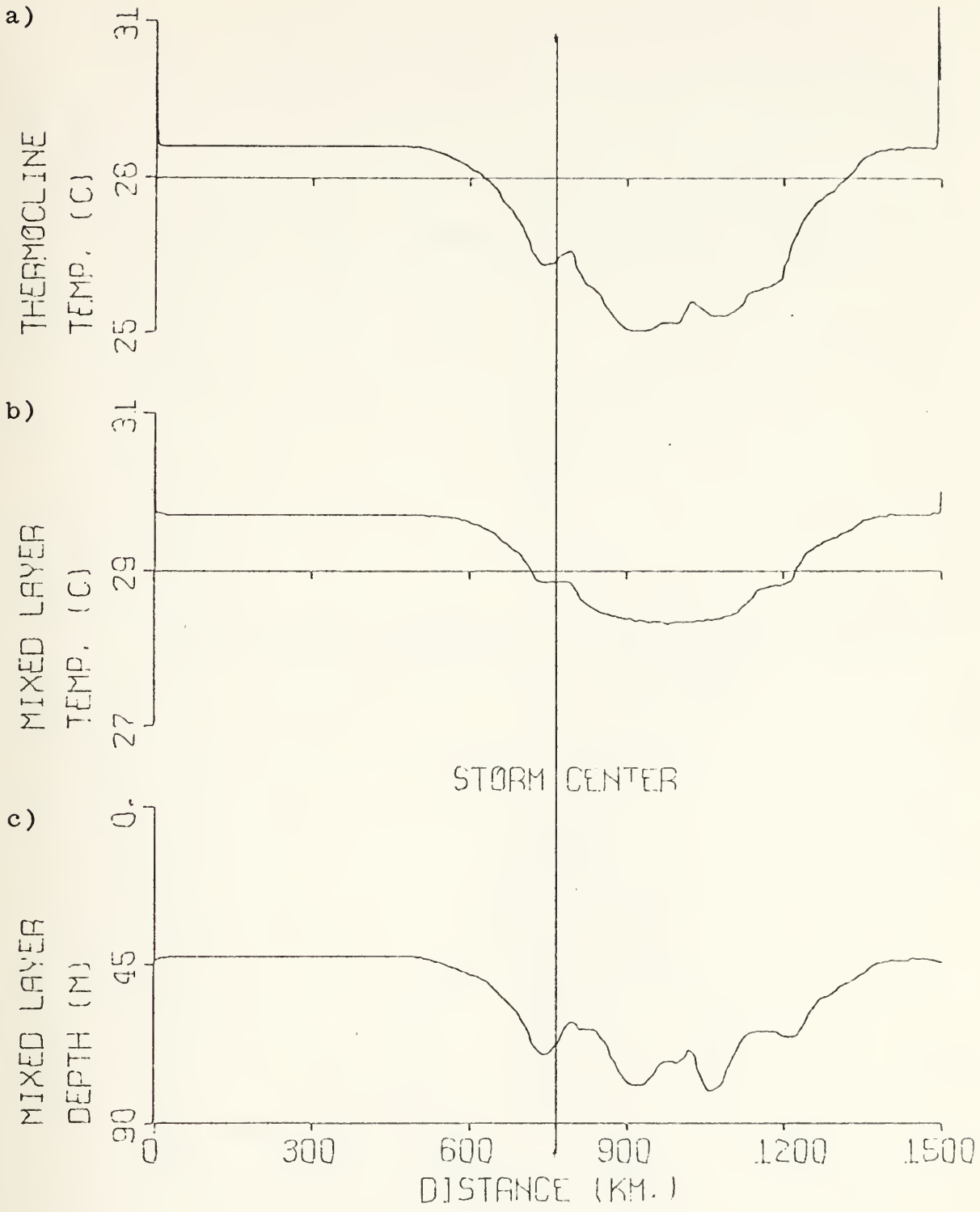

Figure 4. 72 Hour Predicted Values With the Storm Moving at 3.2 kt.

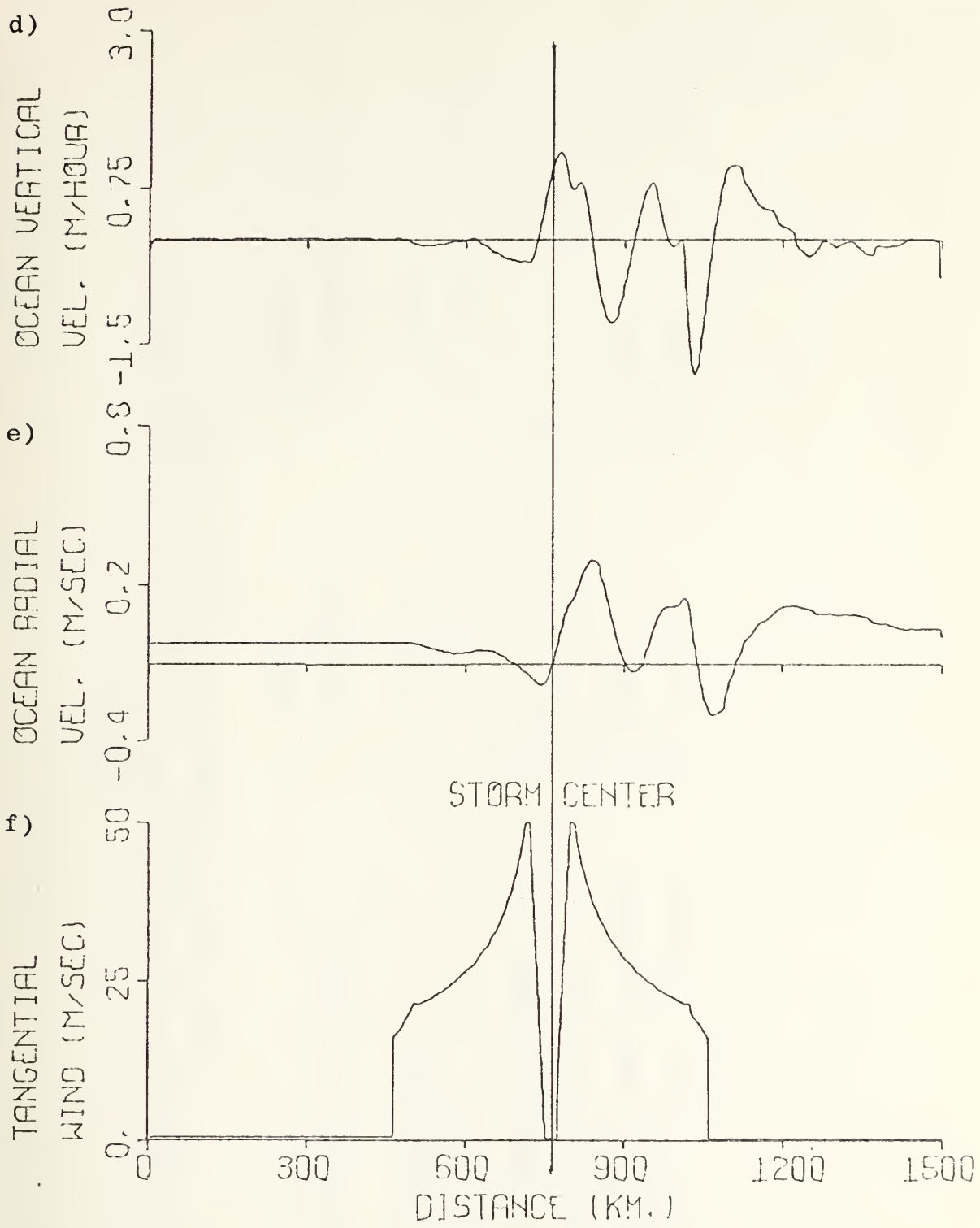

Figure 4. (Cont.) 72 Hour Predicted Values With the Storm Moving at 3.2 kt.

TABLE II

Comparison of Moving Storm Case of Trapnell's Ekman Currents Model and the Dynamic Model, After 18 Hours

	Ekman	Dynamic
Maximum upper level radial current	.28 m/sec^{-1}	.46 m/sec^{-1}
Maximum downwelling	.32 m/hr^{-1}	.45 m/hr^{-1}
Maximum upwelling	3.1 m/hr^{-1}	2.5 m/hr^{-1}
Minimum mixed layer depth	30 m	33 m
Maximum mixed layer depth	61.6 m	68 m
Minimum mixed layer temperature	28.86°C	29.32°C
Maximum mixed layer temperature	30 °C	30 °C

The translation speed of the storm was increased from 3.2 kt to 6.5 kt. In figure 5 the results of integrating this model 36 hours is presented. This can be compared with figure 4 as the same distance has been traveled by the storm but in one-half the time. Note the longer wavelength in the faster storm and also the lag of the upwelling region behind the storm center is much longer in this case. Notice also, comparing 4b and 5b, that less cooling has occurred due to the passage of the faster storm with a minimum mixed-layer temperature of 28.9°C compared with 28.3°C in the slower storm. At the top of the thermocline the same results occur with 26.5°C for the faster storm and 25.0°C for the slower storm. This case was also integrated to 72 hours and these results are presented in figure 6. This will be considered the standard case for the following discussion. Notice that there is little difference compared with the 36 hour case in figure 5, except for the longer wake behind the storm. Temperatures were only slightly lower, by .3°C for the top of the thermocline and .1°C for the mixed layer. The wavelength and magnitude of the variations in mixed-layer depth, vertical velocity, radial velocity and temperature at the top of the thermocline remain essentially the same. This wavelength is approximately 360 km as compared to 180 km in the slower storm.

These results may be compared with the data from Sheets (1974). In the observations the temperature at the interface is higher for greater mixed-layer depths, MLD, and

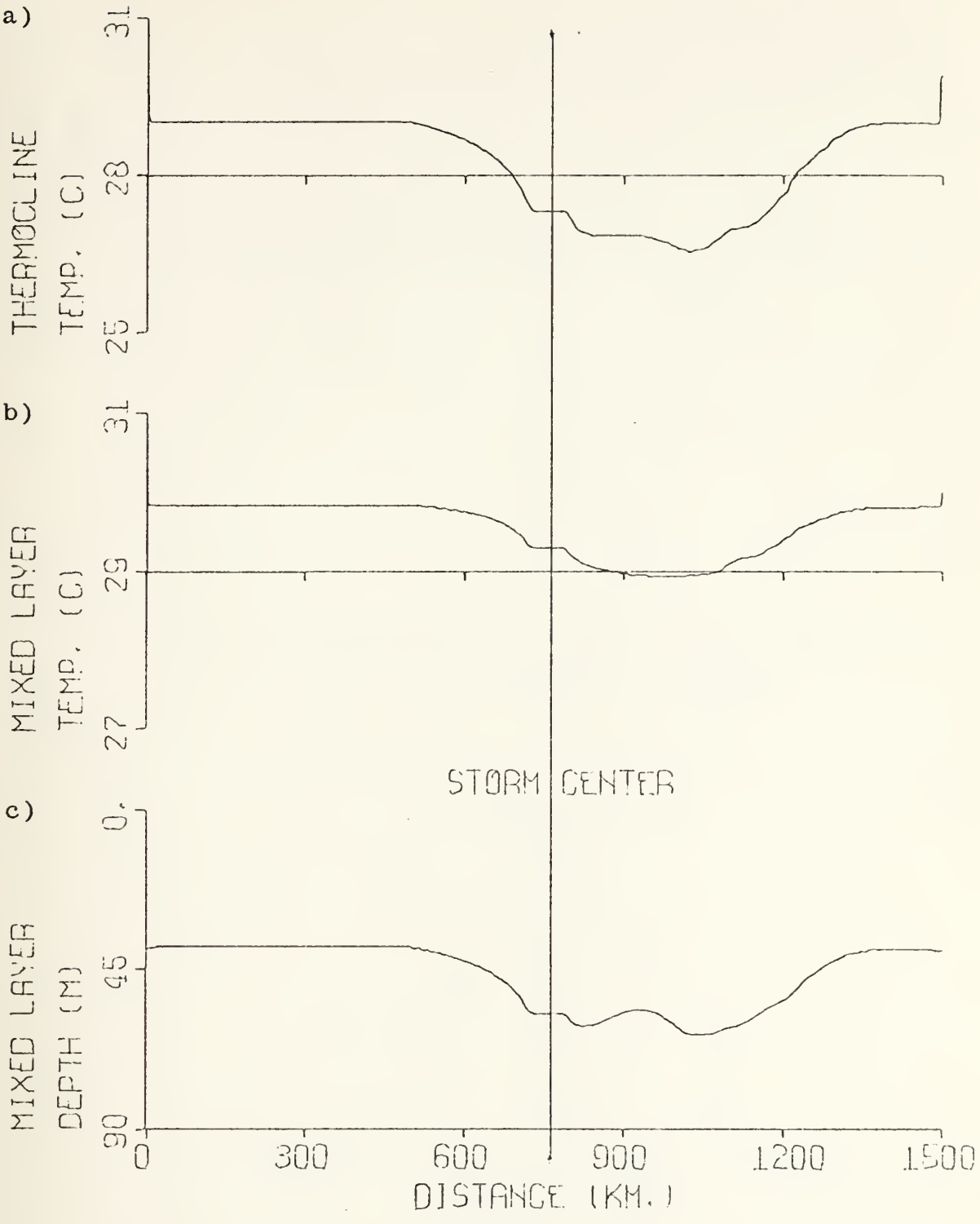

Figure 5. 36 Hour Predicted Values With the Storm Moving at 6.5 kt.

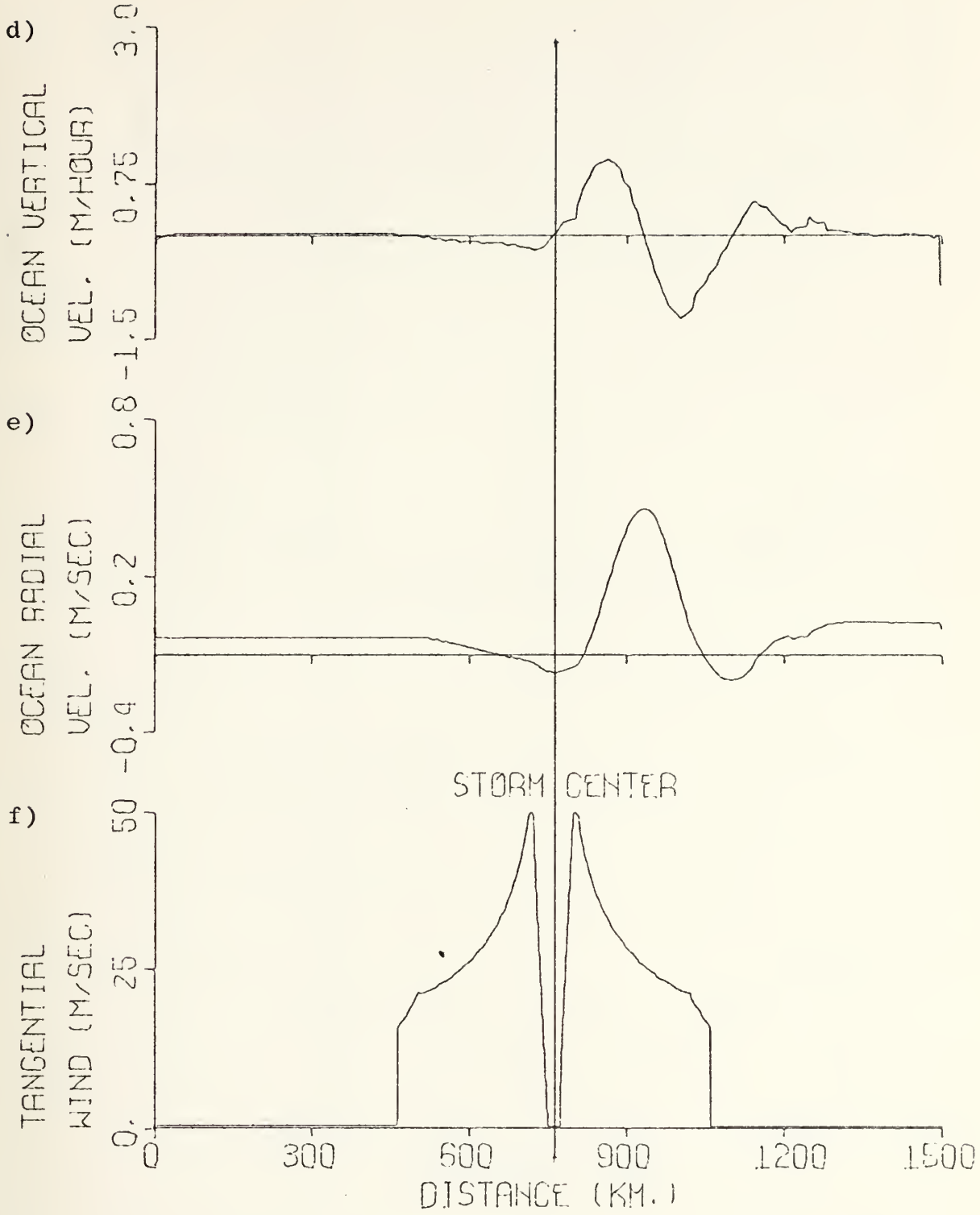

Figure 5. (Cont.) 36 Hour Predicted Values With the Storm Moving at 6.5 kt.

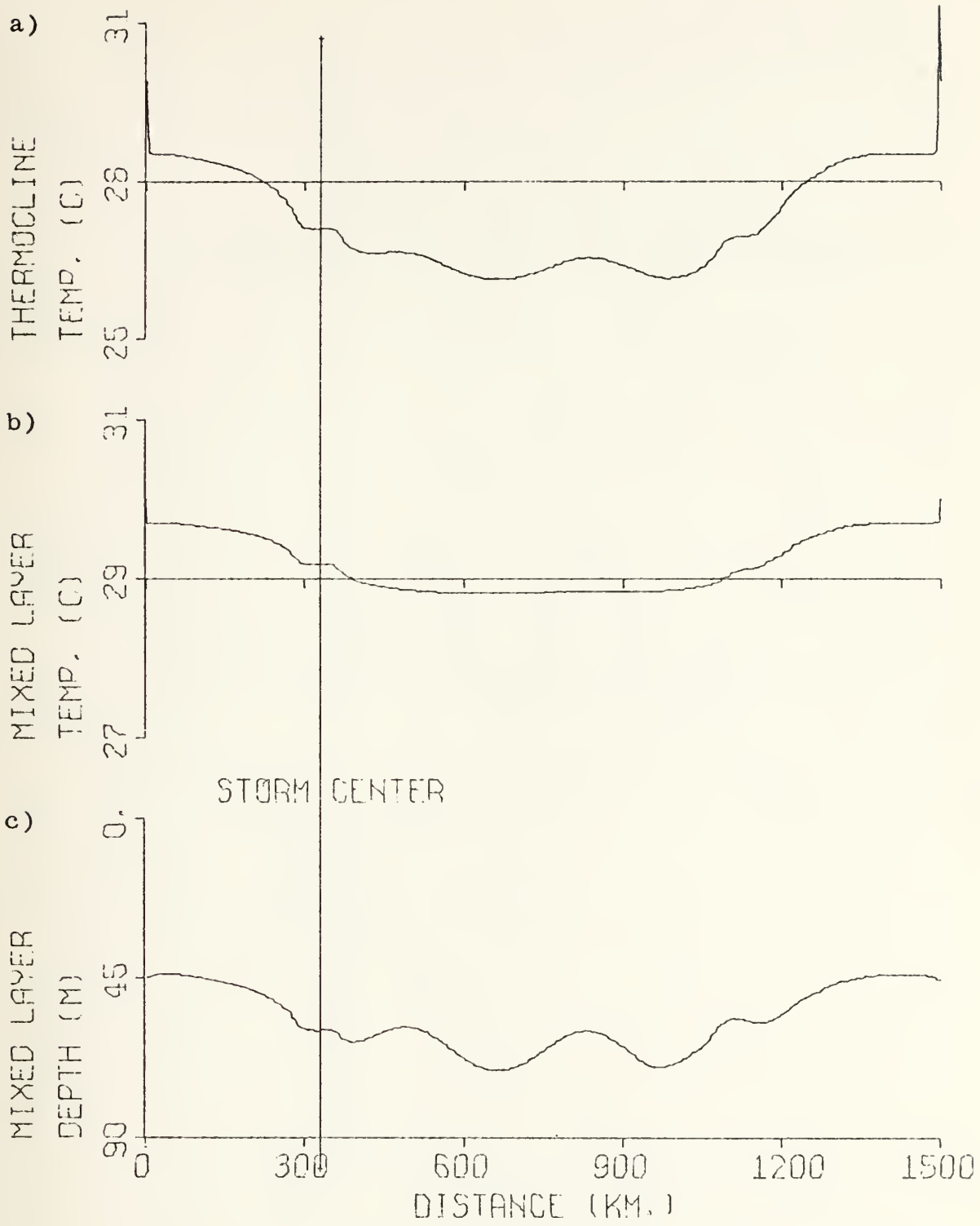

Figure 6. 72 Hour Predicted Values With the Storm Moving at 6.5 kt.

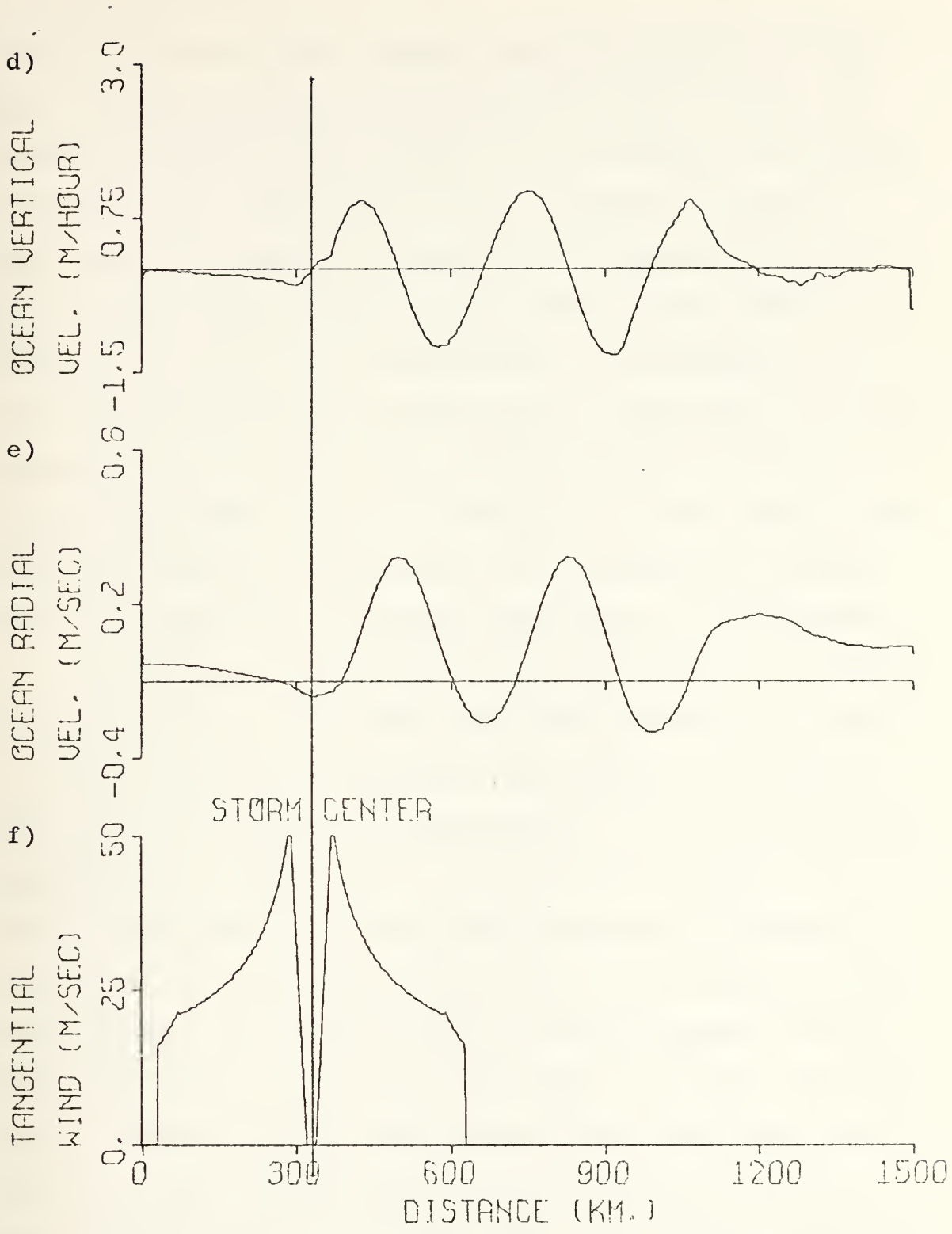

Figure 6. 72 Hour Predicted Values With the Storm (Cont.) Moving at 6.5 kt.

lower for shallow MLD's, which implies that the waves are due to upwelling and downwelling rather than mixing. In figure 7, derived from the data of the standard case we see that this same relationship occurs. However, in Sheets' data these temperature fluctuations also appear within the mixed layer, whereas these fluctuations are not present in figure 6b. Also in the observations the wavelength is on the order of 35 to 40 km which does not agree with the model wavelength of about 360 km. Geisler's theory predicts the longer wavelengths, about 185 km for a 5.2 knot storm. More data with different storm speeds are necessary to compare with the theoretical and model predictions of wavelengths.

The vector contributions to acceleration of currents in both the upper and lower layers are presented in figure 8. These values are computed at the center of the region. The sum of the vectors is proportional to the instantaneous acceleration at that point. The first set of vectors, at 27 hours, represents the ocean condition prior to passage of the storm. At this time the forces are very nearly in balance, except for the lower-level current component normal to the storm track (v_2). The storm passes this point after 37 hours. However, at 36 hours the stresses have been reduced to a very small value compared with the pressure gradient and coriolis terms. It is seen that this sudden reduction, and subsequent reversal of the stress pattern, produces strong inertial waves in the currents. It should also be noted that the phase of the pressure gradient term also

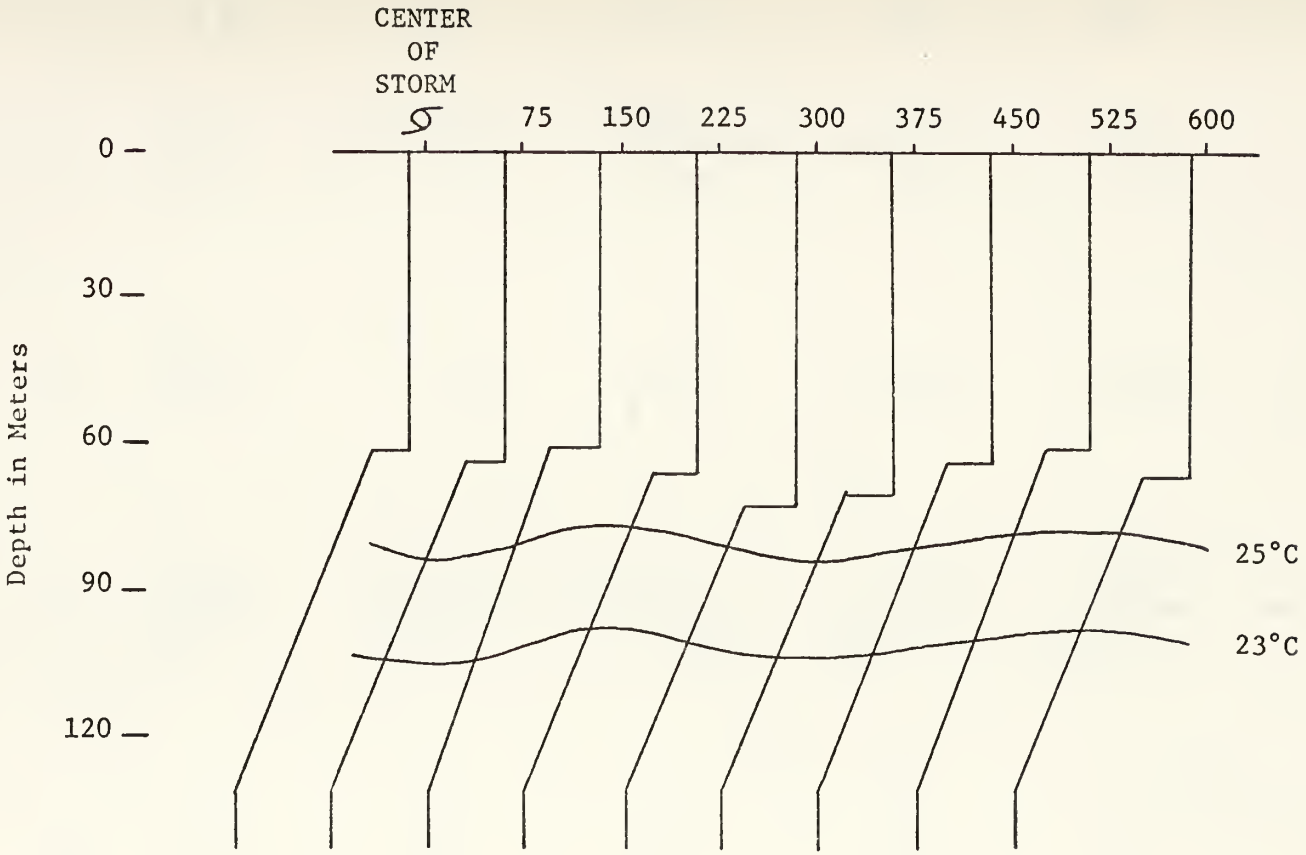

Figure 7. Soundings Produced by the Model from the Center of the Storm to 600 km behind the Storm Spaced at 75 km with the Storm Moving at 6.5 kt for 63 Hours.

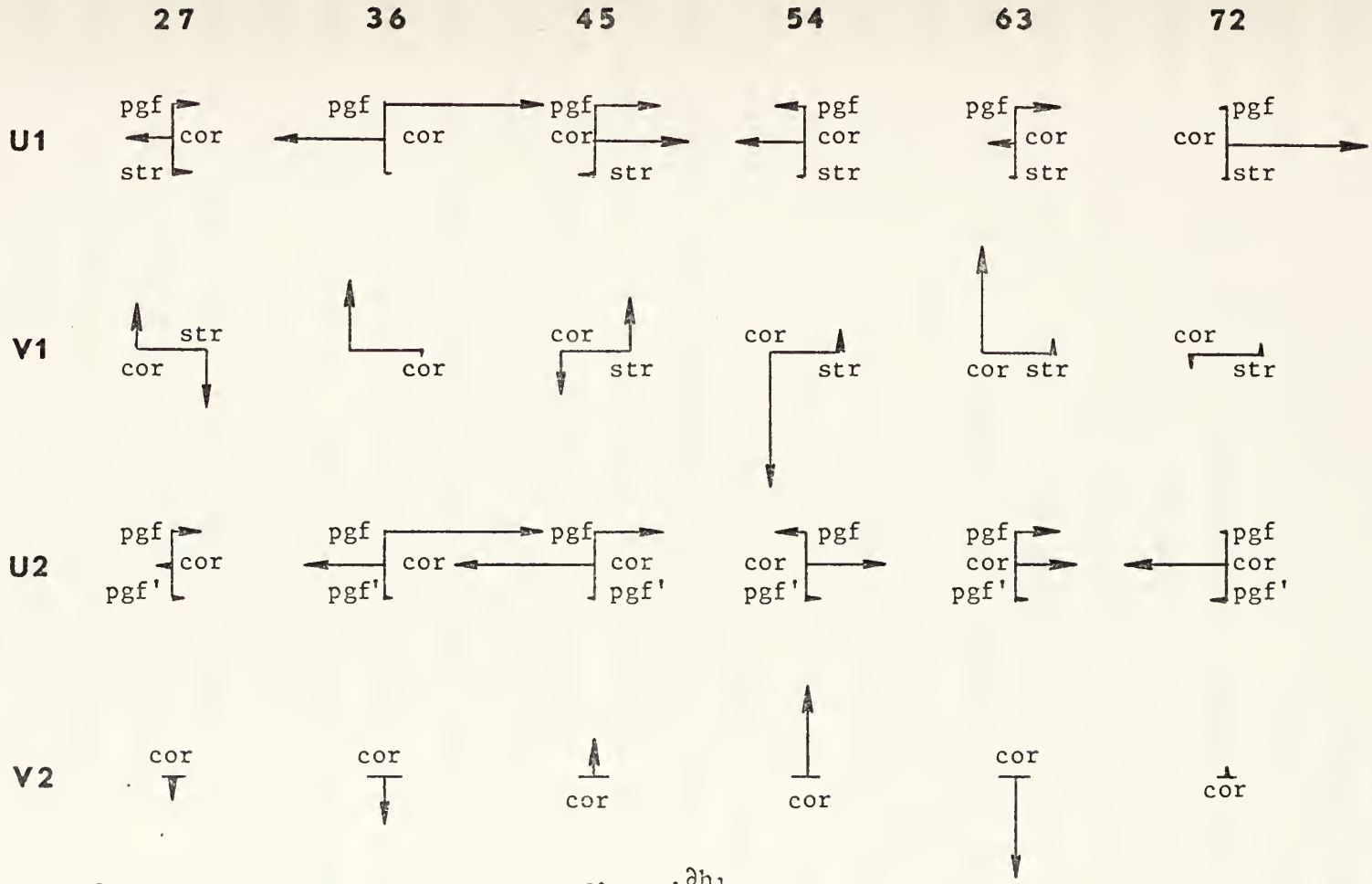

Figure 8. Acceleration Vectors for Currents at the Center of the Grid at Selected Time Steps, with the Storm Moving at 6.5 kt.

contributed to the imbalance of accelerations. At 45 hours this term and the coriolis term are in the same direction, thus contributing to a large imbalance. This condition would not occur without the lag of the pressure gradient term behind the center of the storm. After 45 hours it is seen that the coriolis acceleration dominates the solutions, exchanging kinetic energy between the current components directed parallel (u) and normal (v) to the storm track. To better illustrate this, a hodograph at point 250 of the current direction and magnitude as a function of time is shown in figure 9a. Before the storm passes, the winds are from the top of the figure producing a stress which creates currents from that direction, and due to coriolis there is a current away from the storm center. This is the same behavior noted in the stationary case. In the lower layer the pressure gradient term produces currents toward the center with the coriolis acceleration producing a current component perpendicular to the path of the storm. The storm passes from the right at about 37 hours. The inertial effects are then seen to begin, with the current direction reversed between 36 and 45 hours. Note that the inertial period for the position of the storm, 25°N, is 28.34 hours, and observe that from t=45 hours to t=72 hours, almost one rotation of the current direction has occurred in 27 hours. Therefore we see that inertial effects are very strong, and indeed continue to dominate after the passage of the storm center. Due to this relation to the inertial period, and because the

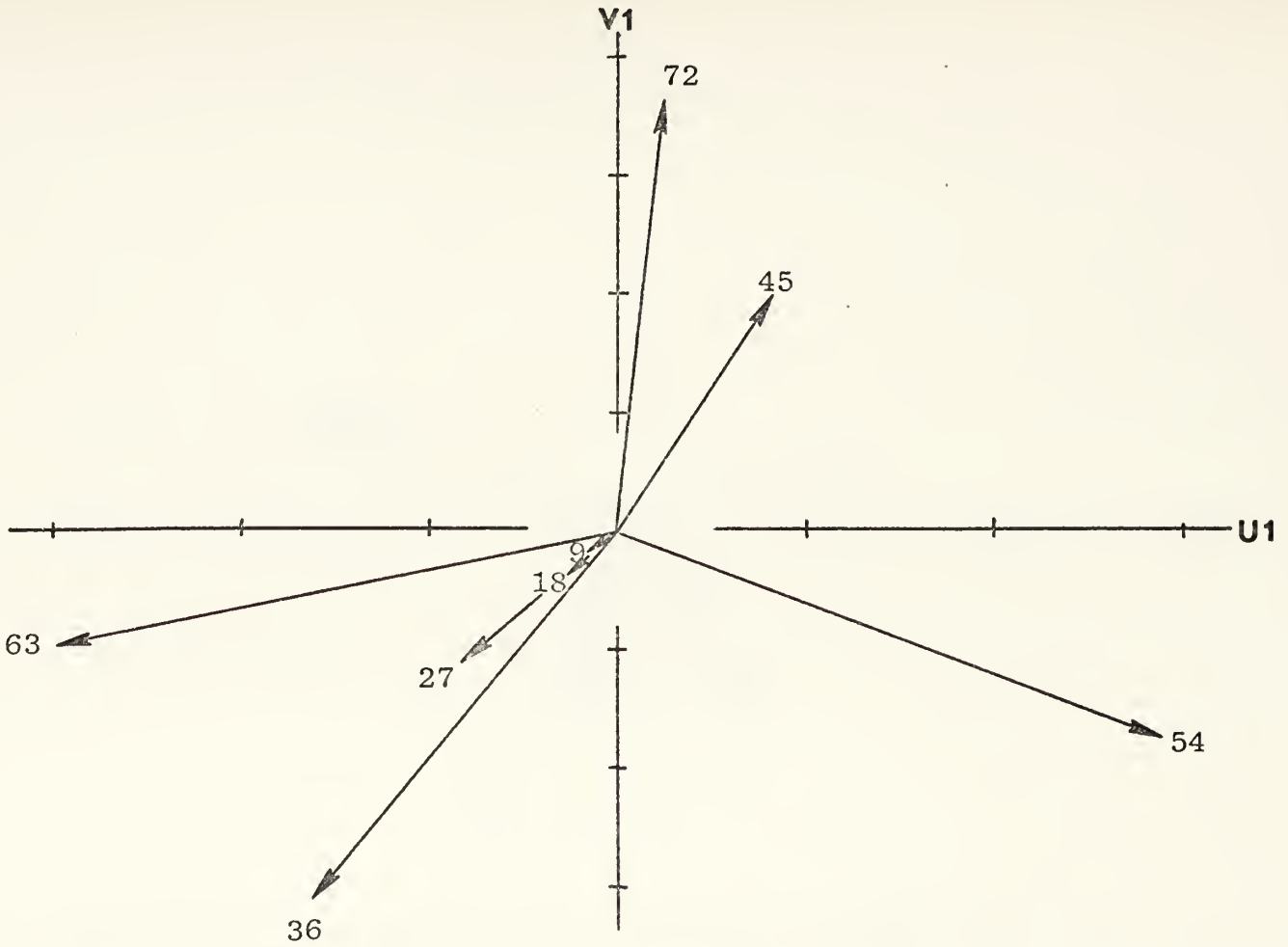

Figure 9a. Hodograph for the Currents at the Center of the Grid, with the Storm Moving at 6.5 kt (the Upper Layer).

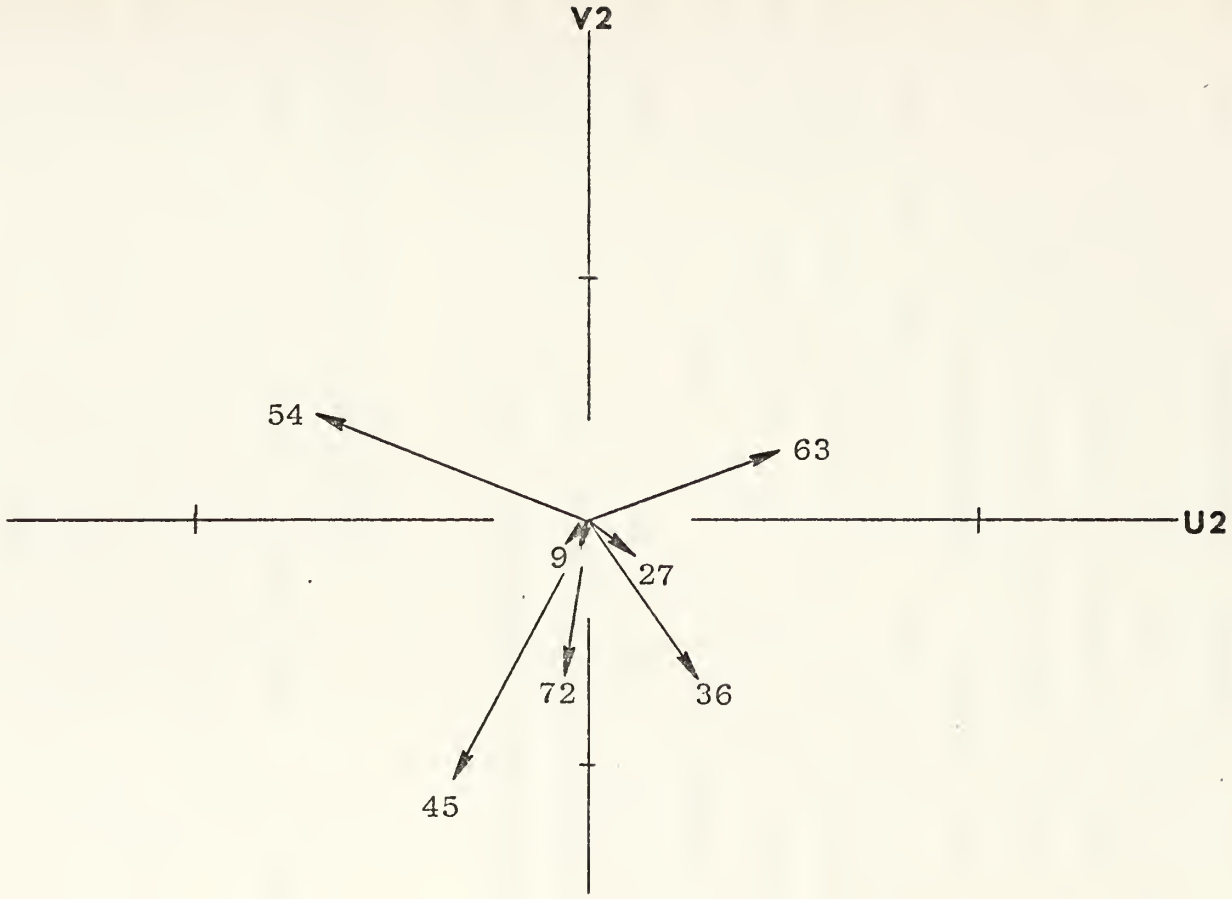

Figure 9b. Hodograph for the Currents at the Center of the Grid, with the Storm Moving at 6.5 kt (the Lower Layer).

waves move with the same speed and direction as the storm, it becomes apparent that the wavelength should be greater for faster moving storms. This relationship is linear in the cases studied here, that is when the storm movement speed is doubled the wavelength is doubled.

A hodograph for the lower layer at this same point and for the same storm speed is presented in figure 9b. The currents in the lower layer have the same features as the upper layer except the magnitudes are smaller and are 180° out of phase with the upper layer. Remembering that the vertical motion is a function of the first derivative of the currents in the lower layer, it is seen that vertical currents are 90° out of phase with the fluctuations of lower layer current parallel to the storm track. This upwelling and downwelling produces the waves at the bottom of the mixed layer, therefore their wavelength is also the same as the fluctuations in currents.

B. VARIATION OF OCEAN PARAMETERS

To check the sensitivity of the model, the standard run was repeated while varying individual parameters. In this section the effects of increased stability in the thermocline layer, increased initial mixed-layer depth, increased stress for currents, and the elimination of the mixing term will be discussed.

Changing the temperature of the undisturbed layer, and hence the temperature at the bottom of the thermocline,

changes the stability of that layer. In this experiment, shown in figure 10, the temperature was lowered to 15°C, thus increasing the stability. The major differences were a slightly cooler mixed layer, about .1°C cooler than the standard model, and a significantly cooler temperature at the top of the thermocline, 1.8°C cooler than the standard case. The reason for the relatively small change in the mixed-layer temperature was that it required more energy to lift the cooler subsurface water into the mixed layer through mixing. The significant reduction in the temperature at the top of the thermocline is due to the cooler water being advected into the region due to the steeper lapse rate (refer to equation (10)). The currents and depths remained essentially the same.

The next variation from the standard case was to initialize the mixed-layer depth at 50 m. These results are shown in figure 11. Due to the larger amount of mass present within the layer due to the increased mixed-layer depth, the velocities in the upper layer were smaller, with a maximum of .36 m sec^{-1} compared to .48 m sec^{-1} for the standard case. Also, the mixed layer was .5°C warmer in this case. Again the wave structure remained unchanged although the overall depth of the mixed layer was increased.

The results of changing the partitioning of surface stress to 70% for current production and 30% for mixing are shown in figure 12. As expected, the currents were stronger in this case than in the standard case of 50% partitioning

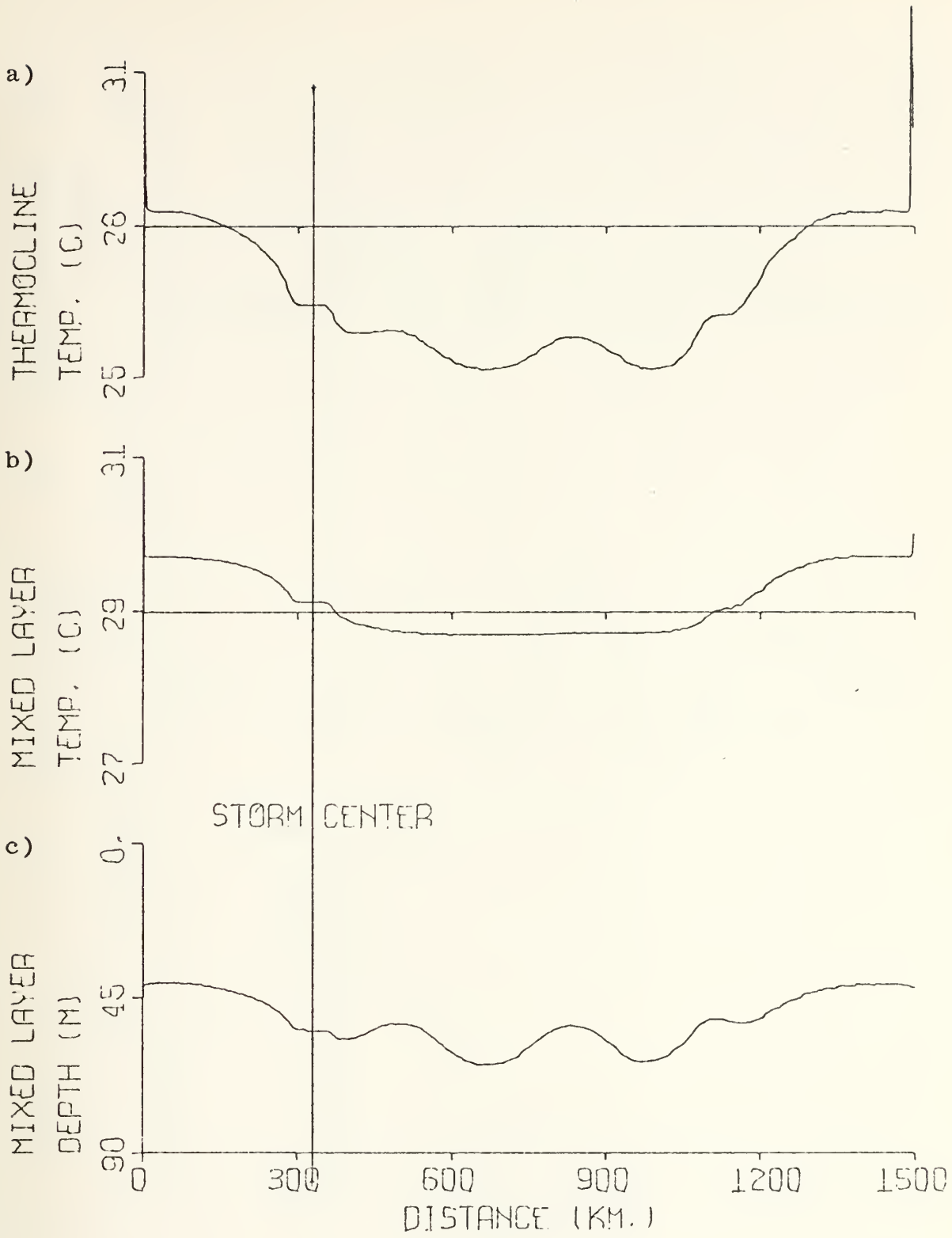

Figure 10. 72 Hour Predicted Values With the Storm Moving at 6.5 kt except with the Initial T_b = 15°C.

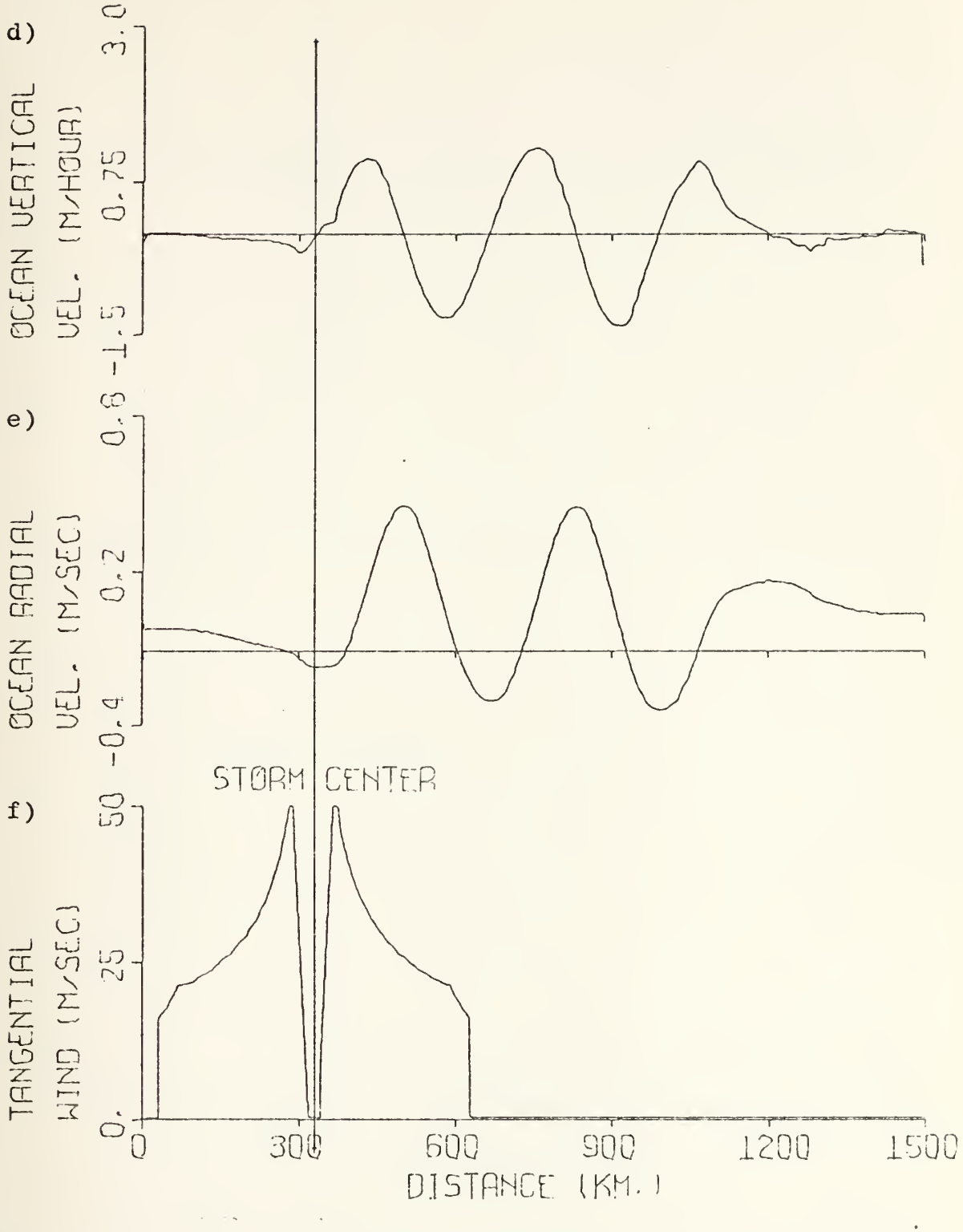

Figure 10. (Cont.) 72 Hour Predicted Values With the Storm Moving at 6.5 kt except with the Initial T_b = 15°C.

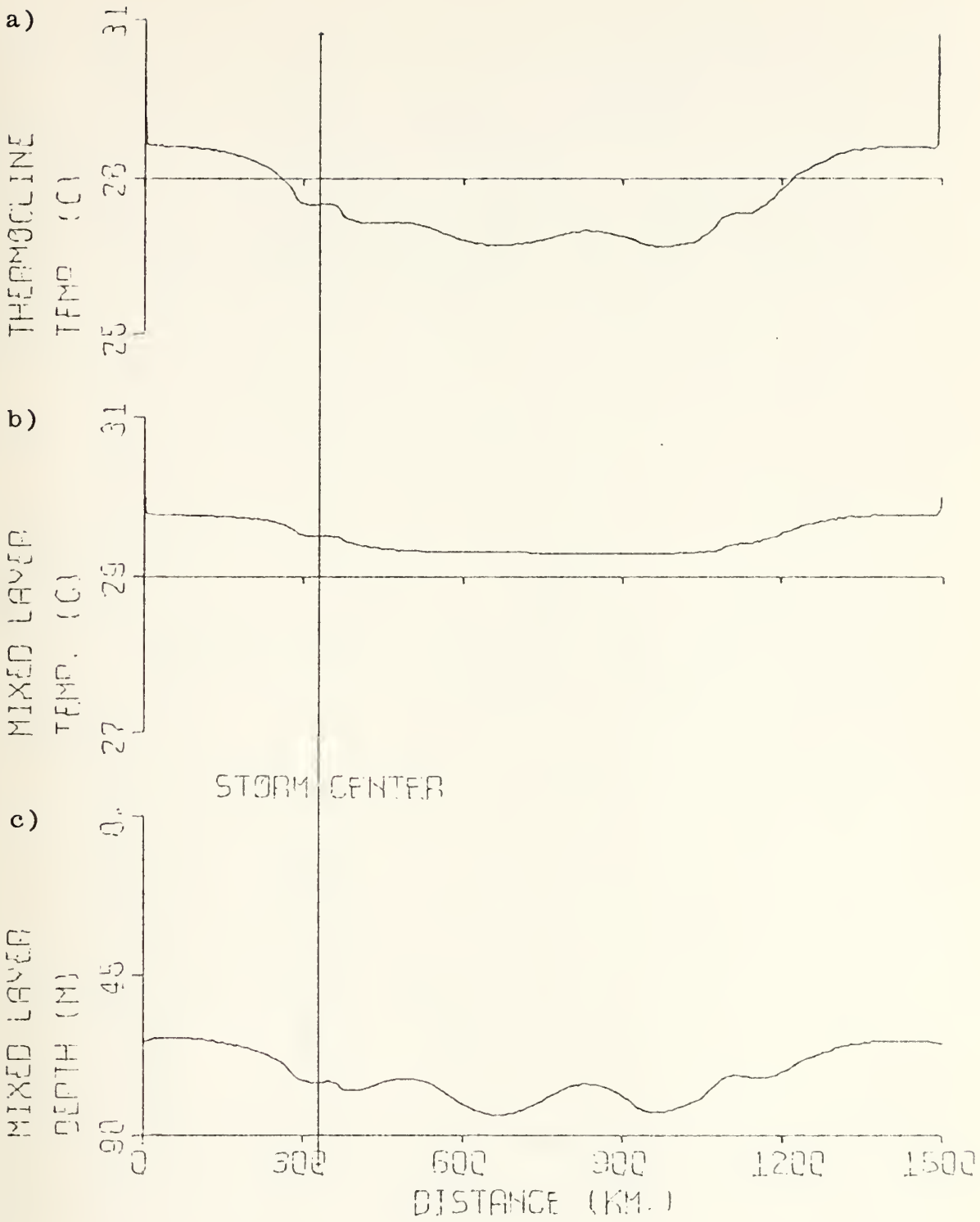

Figure 11. 72 Hour Predicted Values With the Storm Moving at 6.5 kt except Initial h_1 = 50 m.

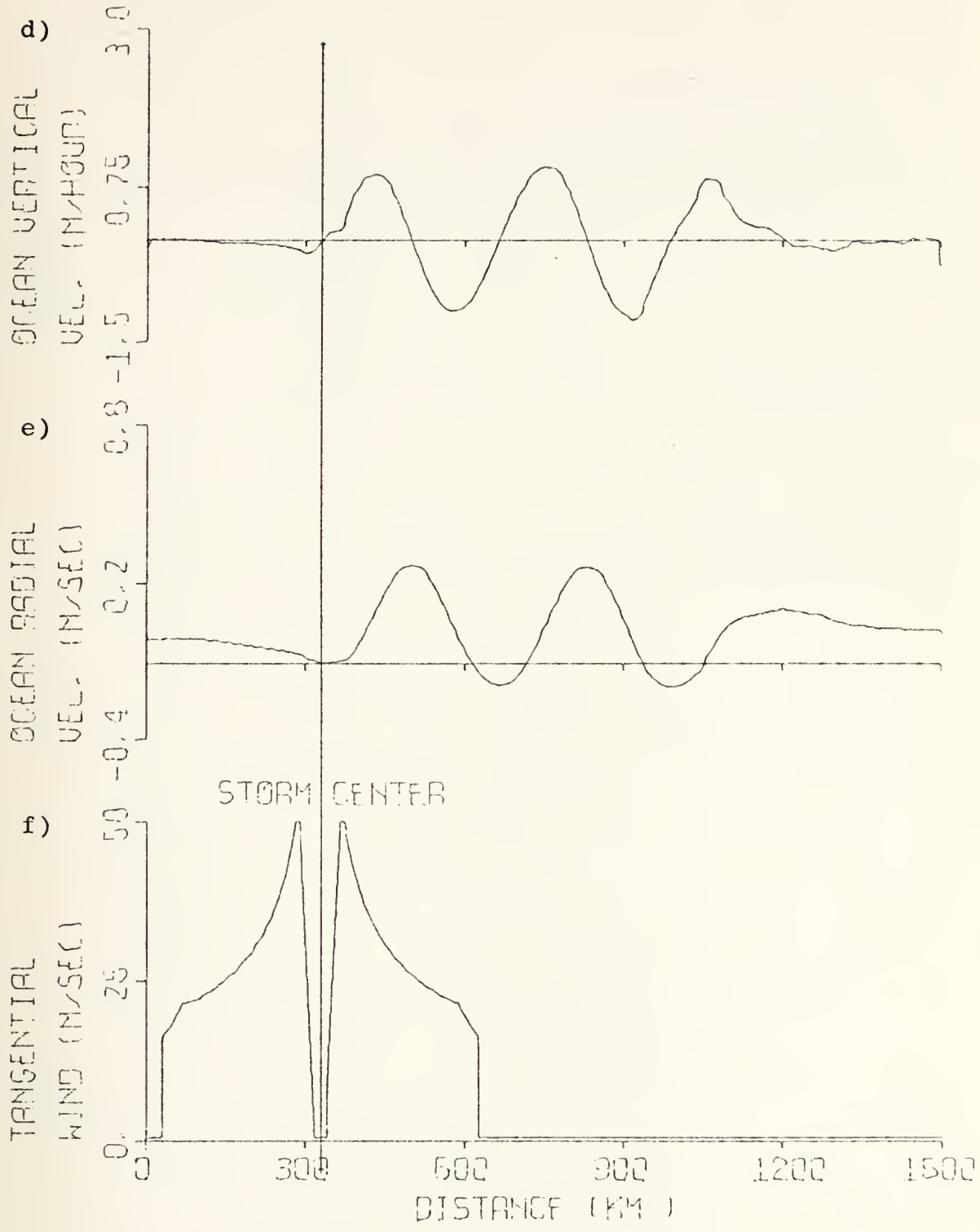

Figure 11. (Cont.) 72 Hour Predicted Values With the Storm Moving at 6.5 kt except Initial h_1 = 50 m.

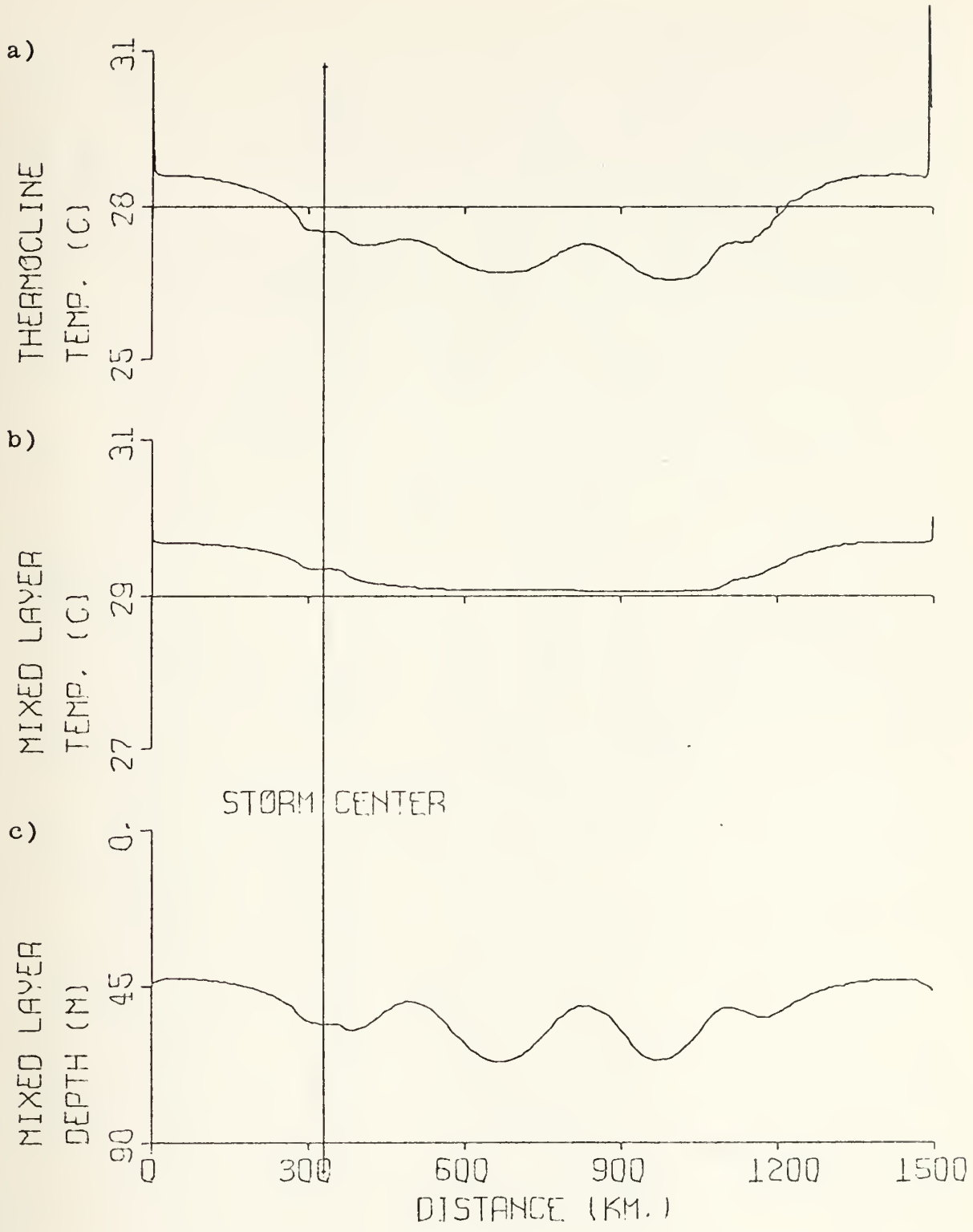

Figure 12. 72 Hour Predicted Values With the Storm Moving at 6.5 kt except partitioning 70% of Surface Stress to Current Production and 30% to Mixing.

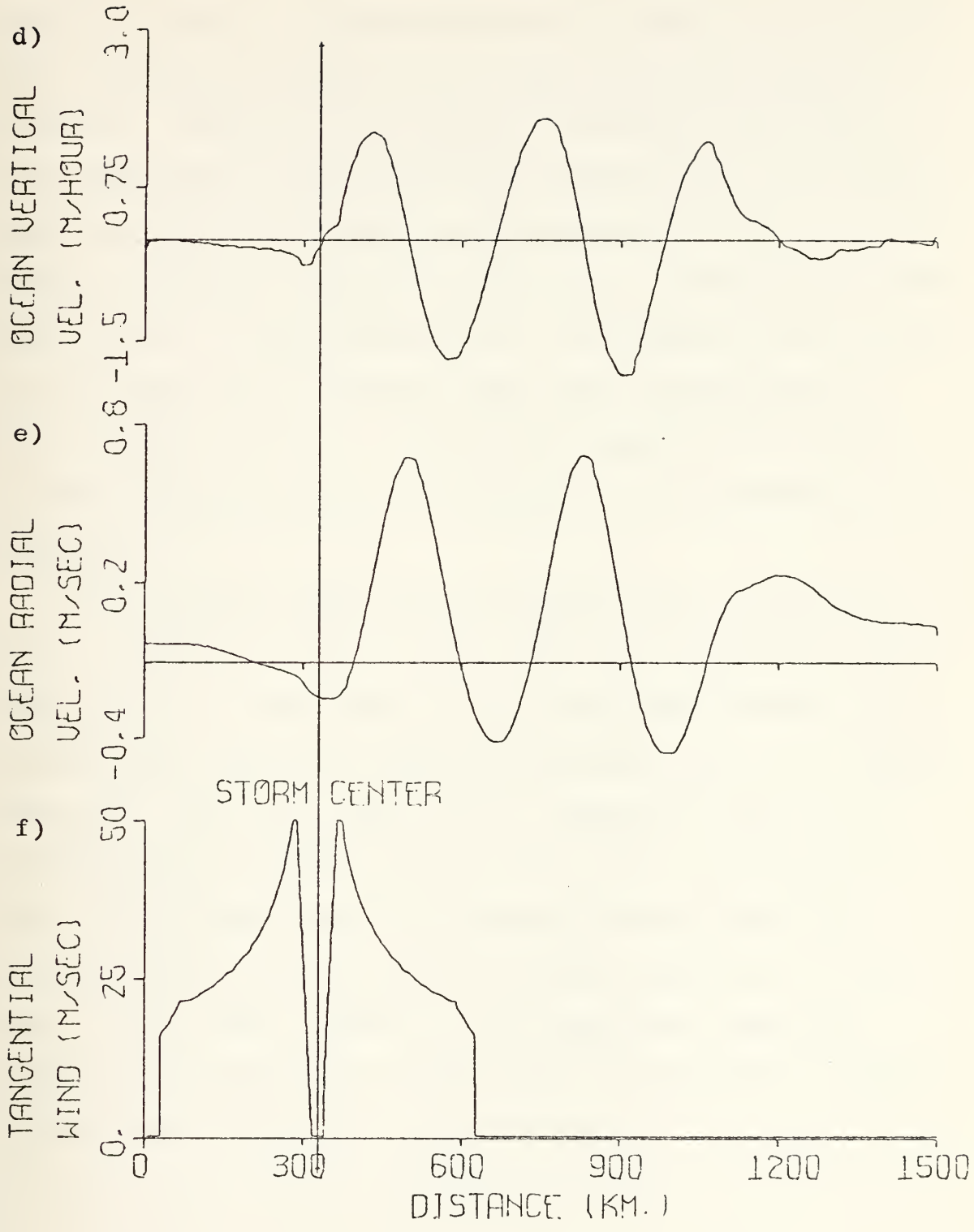

Figure 12. (Cont.) 72 Hour Predicted Values With the Storm Moving at 6.5 kt except partitioning 70% of Surface Stress to Current Production and 30% to Mixing.

shown in figure 6. Comparing figure 6b with 12b it is seen that the surface temperature is lower when the mixing is stronger. Figures 6a and 12a show the same to be true for the temperature at the top of the thermocline. This result and the deeper mixed layer in 6c compared to 12c, show that mixing is the most important contributor to deepening of the mixed layer. A close comparison of the waves at the bottom of the mixed layer, however, shows that the amplitude is increased by about 6 m. It therefore appears that the amplitude of these waves is a function of the magnitude of the currents.

A run was also made with the mixing term set equal to zero. Comparing figure 13 with those of the standard case, figure 6, it is seen that in the case without mixing the surface and thermocline temperatures have only been slightly affected. The mixed layer has not deepened significantly although the waves were present with about the same amplitude. The currents were also stronger even though the stress component partitioned to current production is the same. This effect is due to the mixed layer remaining shallow, and therefore the magnitude of the depth-averaged currents are larger.

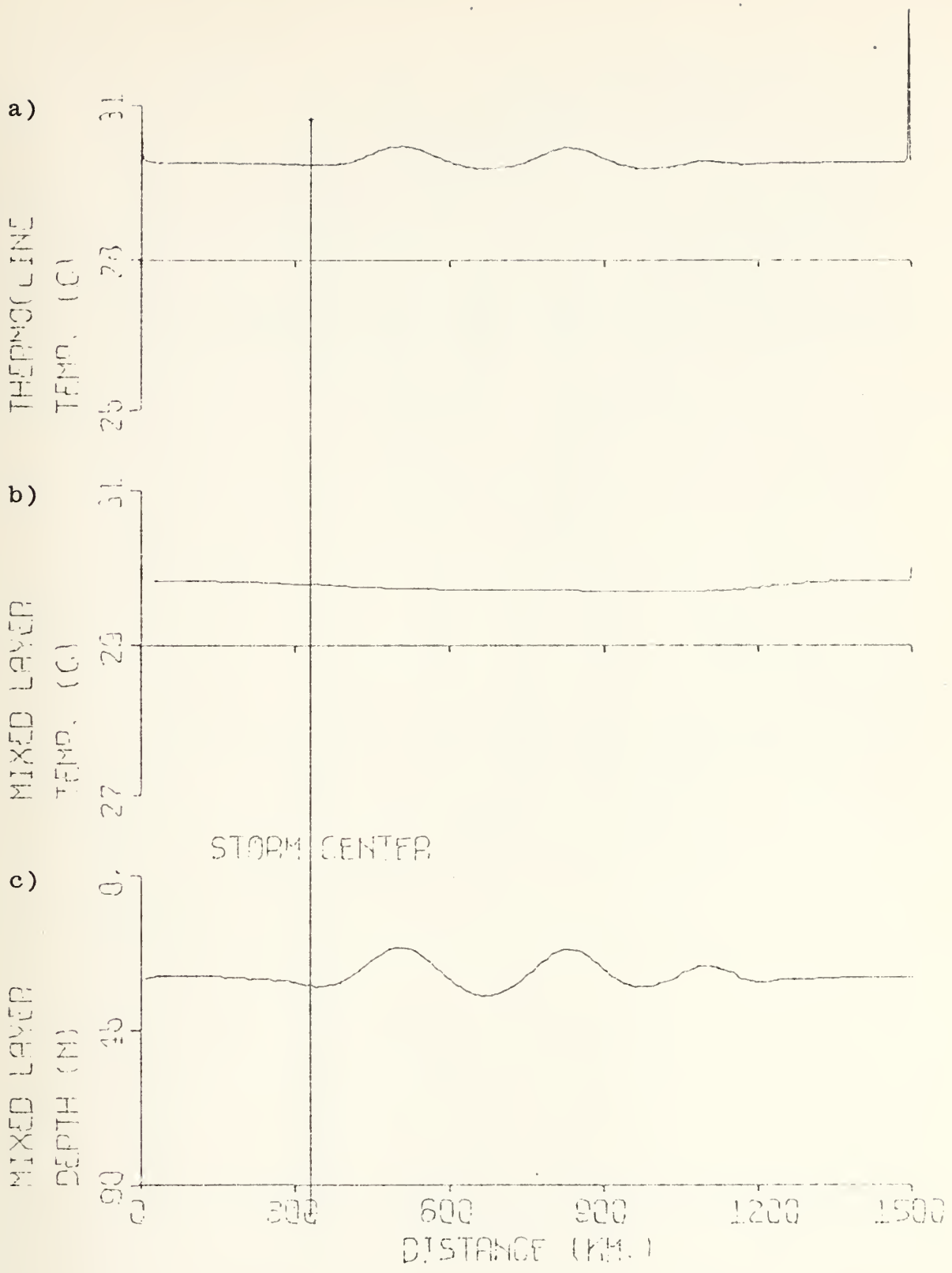

Figure 13. 72 Hour Predicted Values With the Storm Moving at 6.5 kt except Mixing Term is Zero.

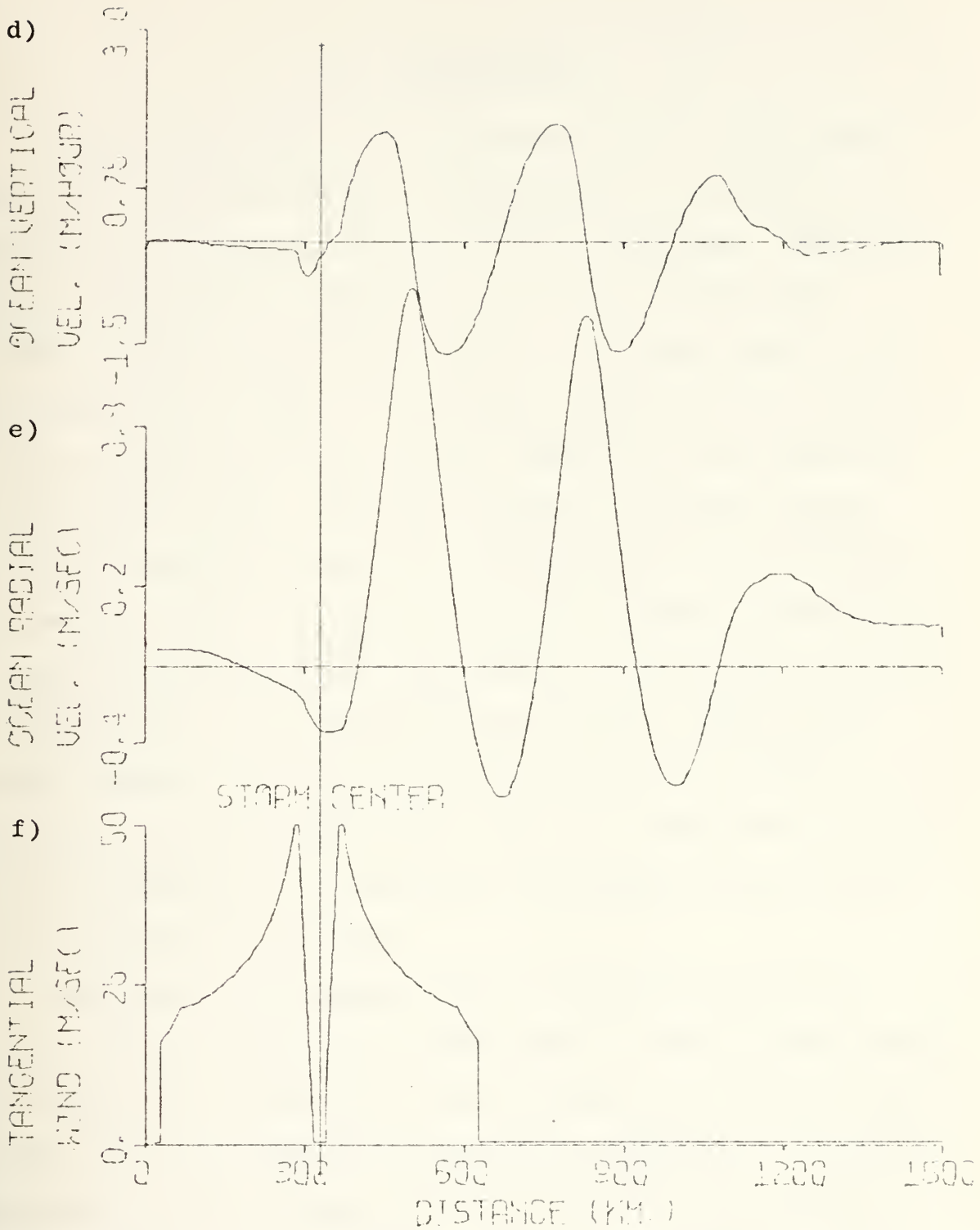

Figure 13. 72 Hour Predicted Values With the Storm Moving (Cont.) at 6.5 kt except Mixing Term is Zero.

IV. CONCLUSIONS

The results shown in the previous section agree quite well with previous theories and observations regarding the behavior of the ocean beneath a moving hurricane. The cooling of the surface temperature, as observed by Leipper (1967), Black and Mallinger (1972), and Sheets (1974), was produced by this model. Entrainment mixing was the dominate factor in cooling of the surface temperature and deepening of the mixed layer. Upwelling maxima and minima as predicted by Geisler (1970) were also produced in the wake of the moving storm. Increased translation speed produced less cooling behind the storm; this agreed with the data of Black and Mallinger. In comparison with Trapnell (1974) this model appears to be quite consistent thermodynamically. However, as stated previously the earlier model did not contain the dynamics to produce the horizontal structure produced by the present model.

The primary discrepancy was the wavelengths of the waves at the bottom of the mixed layer. Sheets shows values on the order of 50 km for a fast moving storm whereas this model shows wavelengths on the order of 360 km for storms moving at 6.5 kt. This difference has not been resolved. In this model these waves appear as a result of inertial waves produced by the sudden change in stress as the storm passes and due to the lag of the pressure gradient force behind the storm center.

In addition to resolving the difference in wavelength mentioned above, other work is necessary on this model. The method of partitioning stress for mixing and current production needs to be studied. Turbulent momentum transfer at the interface should be included. Sensitivity tests should be run on the drag coefficient at the interface and the diffusion constant.

The most valuable refinement would be to extend this model to three dimensions. This would eliminate the most restrictive assumption in this model, axial symmetry. To make this modification, and maintain the present resolution in the most active region, near the hurricane center, would require some type of nested grid arrangement. The nested grid approach would be necessary due to the present limitation of computers in speed and size.

APPENDIX A

SEMI-IMPLICIT SCHEME FOR MOMENTUM AND DEPTH EQUATIONS

The equations in finite difference form which were used in the computer model are developed here. Using the equations presented in the discussion of the model we proceed to implicit solutions, for u_1, u_2, h_1, and h_2. Following the procedure in O'Brien and Hurlburt (1972)

$$\frac{\partial u_1}{\partial t} + g\frac{\partial}{\partial x}(h_1+h_2) = -u_1\frac{\partial u_1}{\partial x} + fv_1 + \frac{(\tau^{S}_{x} - \tau^{I}_{x})}{\rho h_1}$$

$$+A\frac{\partial^2 u_1}{\partial x^2} \equiv U_1 \qquad \text{(A-1)}$$

$$\frac{\partial h_1}{\partial t} + H_1\frac{\partial u_1}{\partial x} = -h_1'\frac{\partial u_1}{\partial x} - u_1\frac{\partial h_1}{\partial x} + M \equiv D_1 \qquad \text{(A-2)}$$

$$\frac{\partial u_2}{\partial t} + g\frac{\partial}{\partial x}(h_1+h_2) - g'\frac{\partial h_1}{\partial x} = -u_2\frac{\partial u_2}{\partial x} + fv_2 + \frac{\tau^{I}_{x}}{\rho h_2}$$

$$+A\frac{\partial^2 u_2}{\partial x^2} \equiv U_2 \qquad \text{(A-3)}$$

$$\frac{\partial h_2}{\partial t} + H_2\frac{\partial u_2}{\partial x} = -h_2'\frac{\partial u_2}{\partial x} - u_2\frac{\partial h_2}{\partial x} - M \equiv D_2 \qquad \text{(A-4)}$$

The tendencies are now evaluated for a $2\Delta t$ time step and the divergence terms are averaged between time levels $(n-1)\Delta t$ and $(n+1)\Delta t$. The subscript j is the space index while the superscript n is the time index.

$$u_{1j}^{n+1}+[\Delta tg\frac{\partial}{\partial x}(h_1+h_2)]_j^{n+1} = 2\Delta tU_{1j}^{n}+u_{1j}^{n-1}-[\Delta tg\frac{\partial}{\partial x}(h_1+h_2)]_j^{n-1}$$

$$\equiv L_1 \qquad \text{(A-5)}$$

$$h_{1j}^{n+1}+[\Delta tH_1\frac{\partial u_1}{\partial x}]_j^{n+1} = 2\Delta tD_{1j}^{n}+h_{1j}^{n-1}-[\Delta tH_1\frac{\partial u_1}{\partial x}]_j^{n-1} \equiv L_2 \qquad \text{(A-6)}$$

$$u_{2j}^{n+1}+[\Delta tg\frac{\partial}{\partial x}(h_1+h_2)-\Delta tg'\frac{\partial h_1}{\partial x}]_j^{n+1} = 2\Delta tU_{2j}^{n}+u_{2j}^{n-1}$$

$$-[\Delta tg\frac{\partial}{\partial x}(h_1+h_2)-\Delta tg'\frac{\partial h_1}{\partial x}]_j^{n-1} \equiv L_3 \qquad \text{(A-7)}$$

$$h_{2j}^{n+1}+[\Delta tH_2\frac{\partial u_2}{\partial x}]_j^{n+1} = 2\Delta tD_{2j}^{n}+h_{2j}^{n-1}-[\Delta tH_2\frac{\partial u_2}{\partial x}]_j^{n-1} \equiv L_4 \qquad \text{(A-8)}$$

With homogeneous boundary conditions on u_1 and u_2, h_1 and h_2 can be eliminated. Substituting (A-6) and (A-8) into (A-5) and (A-7) respectively, and dropping the n+1 superscript the following is obtained.

$$u_{1j}+\{\Delta tg\frac{\partial}{\partial x}[L_2-(\Delta tH_1\frac{\partial u_1}{\partial x})+L_4-(\Delta tH_2\frac{\partial u_2}{\partial x})]\}_j = L_1 \qquad \text{(A-9)}$$

$$u_{2j}+\{\Delta tg\frac{\partial}{\partial x}[L_2-(\Delta tH_1\frac{\partial u_1}{\partial x})+L_4-(\Delta tH_2\frac{\partial u_2}{\partial x})]$$

$$-\Delta tg'\frac{\partial}{\partial x}[L_2-(\Delta tH_1\frac{\partial u_1}{\partial x})]\}_j = L_3 \qquad \text{(A-10)}$$

Expanding (A-9) gives:

$$u_{1j}-(\Delta t)^2g[H_1\frac{\partial}{\partial x}(\frac{\partial u_1}{\partial x})+H_2\frac{\partial}{\partial x}(\frac{\partial u_2}{\partial x})] = L_1-\Delta tg\frac{\partial}{\partial x}(L_2+L_4) \qquad \text{(A-11)}$$

Expanding (A-10) gives:

$$u_{2j}-(\Delta t)^2 g[H_1\frac{\partial}{\partial x}(\frac{\partial u_1}{\partial x})+H_2\frac{\partial}{\partial x}(\frac{\partial u_2}{\partial x})]+g'(\Delta t)^2 H_1\frac{\partial}{\partial x}(\frac{\partial u_1}{\partial x})$$

$$= L_3-\Delta tg[\frac{\partial}{\partial x}(L_2+L_4)]+\Delta tg'\frac{\partial L_2}{\partial x} \qquad \text{(A-12)}$$

Subtracting (A-11) from (A-12) gives:

$$u_{2j}-u_{1j}+g'(\Delta t)^2 H_1\frac{\partial}{\partial x}(\frac{\partial u_1}{\partial x}) = L_3-L_1+\Delta tg'\frac{\partial L_2}{\partial x} = e \qquad \text{(A-13)}$$

Substituting u_{1j} from (A-13) into (A-11) gives:

$$u_{2j}-(\Delta t)^2[(g-g')H_1\frac{\partial}{\partial x}(\frac{\partial u_1}{\partial x})]-g(\Delta t)^2 H_2\frac{\partial}{\partial x}(\frac{\partial u_2}{\partial x})$$

$$= L_3-\Delta tg\frac{\partial}{\partial x}(L_2+L_4)+\Delta tg'\frac{\partial L_2}{\partial x} \equiv d \qquad \text{(A-14)}$$

For the remainder of this derivation only, the following definitions are made.

$a \equiv gH_1(\Delta t)^2$

$b \equiv gH_2(\Delta t)^2$

$c \equiv g'H_1(\Delta t)^2$

$f \equiv 1/(\Delta x)^2$

From (A-13) we get

$$u_{2j}-u_{1j}+c\frac{\partial^2 u_1}{\partial x^2} = e \qquad \text{(A-15)}$$

From (A-14) we get

$$u_{2j}-(a-c)\frac{\partial^2 u_1}{\partial x^2} - b\frac{\partial^2 u_2}{\partial x^2} = d \qquad \text{(A-16)}$$

Using $\frac{\partial^2 u}{\partial x^2} = \frac{u_{j+1}-2u_j+u_{j-1}}{(\Delta x)^2}$ Eq. (A-15) becomes

$$u_{2j}-u_{1j}+cf(u_{1j+1}-2u_{1j}+u_{1j-1}) = e \qquad \text{(A-17)}$$

$$-u_{1j+1}+(2+\frac{1}{cf})u_{1j}-u_{1j-1} = \frac{u_{2j}-e}{cf} \qquad \text{(A-18)}$$

This is the form to apply the method presented in Richtmyer (1967). Using the symbol conventions in that text,

$$A = 1$$

$$B = (2 + \frac{1}{cf})$$

$$C = 1$$

$$D = (u_{2j}-e_j)/cf$$

As c and f are both positive the criterion, explained in Richtmyer, of B>A+C is satisfied.

Having used a guess for u_{2j} above, a new u_{2j} using the above u_{1j} can now be computed from Eq. (A-10).

$$-u_{2j+1}+(2+\frac{1}{fb})u_{2j}-u_{2j-1} = \frac{d}{fb} + \frac{a-c}{b}(u_{1j+1}-2u_{1j}+u_{1j-1}) \qquad \text{(A-19)}$$

As used for u_1

$$A = 1$$

$$B = 2 + \frac{1}{fb}$$

$$C = 1$$

$$D = \frac{d}{fb} + \frac{a-c}{b}(u_{1j+1}-2u_{1j}+u_{1j-1})$$

Solve Eq. (A-18) and (A-19) iteratively to obtain values for u_1 and u_2.

The scheme in Richtmyer is

$$u_j = E_j u_{j+1} + F_j \tag{A-20}$$

where

$$E_j = \frac{A_j}{B_j - C_j E_{j-1}} = \frac{1}{B_j - E_{j-1}} \tag{A-21}$$

and

$$F_j = \frac{D_j + F_{j-1}}{B_j - E_{j-1}} \tag{A-22}$$

The boundary conditions, u_1, u_2, E_0, and F_0, are zero.

Values for h_{1j} are obtained by rearranging Eq. (A-6)

$$h_{1j}^{n+1} = L_2 - [\Delta t H_1 \frac{\partial u_1}{\partial x}]_j^{n+1} \tag{A-23}$$

Likewise Eq. (A-8) provides a relationship for h_{2j}.

$$h_{2j}^{n+1} = L_4 - [\Delta t H_2 \frac{\partial u_2}{\partial x}]_j^{n+1} \tag{A-24}$$

This completes the semi-implicit scheme used in computing new values for u_1, u_2, h_1 and h_2.

The remainder of the equations are handled explicitly, using centered differences in time and space.

BIBLIOGRAPHY

1. Black, P.G., and Mallinger, W.D., The Mutual Interaction of Hurricane Ginger and the Upper Mixed Layer of the Ocean. 1971 Project Stormfury Annual Report, Dept. of Commerce, 63-87, 1972.

2. Blackadar, A.K., 1965: A Simplified Two-Layer Model of the Baroclinic Neutral Atmosphere Boundary Layer. Air Force Cambridge Research Laboratories Report 65-531, pp. 49-65.

3. Cardone, V.J., 1969: Specification of the Wind Distribution in the Marine Boundary Layer for Wave Forecasting. New York University, School of Engineering and Science, Scientific Report GSL-TR69-1, University Heights, New York.

4. Denman, K.L., 1973: A Time-Dependent Model of the Upper Ocean, Journal of Physical Oceanography, 3, pp. 173-184.

5. Elsberry, R.L., Pearson, N.A.S., and Corgnati, L.B., 1974: A Quasi-Empirical Model of the Hurricane Boundary Layer, Journal of Geophysical Research, 79, pp. 3033-3040.

6. Federov, K.N., 1973: The Effect of Hurricanes and Typhoons on the Upper Active Ocean Layers, Oceanology, 12, pp. 329-332.

7. Fraim, T.S., 1973: Oceanic Thermal Response to a Time-Dependent Hurricane Model, M.S. Thesis, Naval Postgraduate School, Monterey, California.

8. Geisler, J.E., 1970: Linear Theory of the Response of a Two Layer Ocean to a Moving Hurricane, Geophysical Fluid Dynamics, 1, pp. 249-272.

9. Gray, W.M. and Shea, D.J., 1973: The Hurricanes' Inner Core Region, 2, Thermal Stability and Dynamic Characteristics, J. Atmos. Sci., 30, pp. 1565-1576.

10. Haltiner, G.J., 1971: Numerical Weather Prediction, John Wiley and Sons, Inc., New York, 317 pp.

11. Kraus, E.B., and Turner, J.S., 1967: A One-Dimensional Model of the Seasonal Thermocline, Tellus, 19, pp. 88-106.

12. Kwizak, M. and Robert, A., 1971: A Semi-Implicit Scheme for Grid Point Atmospheric Models of the Primitive Equations, Mon. Wea. Rev., 99, pp. 32-36.

13. Leipper, D.F., 1967: Observed Ocean Conditions and Hurricane Hilda, 1964, J. Atmos. Sci., 24, pp. 182-196.

14. O'Brien, J.J., 1967: The Non-Linear Response of a Two-Layer, Baroclinic Ocean to a Stationary, Axially-Symmetric Hurricane: Part II, J. Atmos. Sci., 24, pp. 208-215.

15. O'Brien, J.J., 1968: The Response of the Ocean to a Slowly Moving Cyclone, NCAR Manuscript No. 68-57, 36 pp.

16. O'Brien, J.J., and Hurlburt, H.E., 1972: A Numerical Model of Coastal Upwelling, Journal of Physical Oceanography, 2, pp. 14-26.

17. O'Brien, J.J. and Reid, R.O., 1967: The Non-Linear Response of a Two-Layer, Baroclinic Ocean to a Stationary, Axially - Symmetric Hurricane; Part I, J. Atmos. Sci., 24, pp. 197-207.

18. Richtmyer, R.D., and Morton, K.W., 1967: Difference Methods for Initial-Value Problems, Interscience Publishers, New York, pp. 198-201.

19. Riehl, H., 1963: Some Relations Between Wind and Thermal Structure of Steady-State Hurricanes, J. Atmos. Sci., 20, pp. 276-387.

20. Sheets, R.C., 1974: Unique Data Set Obtained in Hurricane Ellen (1973), Bulletin of the American Meteorological Society, 55, no. 2, pp. 144-146.

21. Trapnell, R.N., Jr., 1974: Ocean Thermal Response to a Moving Hurricane Model, M.S. Thesis, Naval Postgraduate School, Monterey, California.

INITIAL DISTRIBUTION LIST

		No. Copies
1.	Defense Documentation Center Cameron Station Alexandria, Virginia 22314	2
2.	Library, Code 0212 Naval Postgraduate School Monterey, California 93940	2
3.	Department Chairman, Code 51 Department of Meteorology Naval Postgraduate School Monterey, California 93940	1
4.	Professor R. L. Elsberry, Code 51Es Department of Meteorology Naval Postgraduate School Monterey, California 93940	8
5.	Professor D. F. Leipper, Code 58Lr Department of Oceanography Naval Postgraduate School Monterey, California 93940	1
6.	Professor R. L. Haney, Code 51Hy Department of Meteorology Naval Postgraduate School Monterey, California 93940	1
7.	LT Stanley H. Grigsby, USN FLEWEACEN GUAM COMNAVMARIANAS Box 12 FPO San Francisco 96630	2
8.	Commander Naval Weather Service Command Headquarters Naval Weather Service Command Washington Navy Yard Washington, D.C. 20390	1
9.	Office of Naval Research Code 480 Arlington, Virginia 22217	1
10.	Library, Code 3330 Naval Oceanographic Office Washington, D.C. 20373	1

No. Copies

11. Commanding Officer 1
Fleet Numerical Weather Central
Monterey, California 93940

12. Commanding Officer 1
Environmental Prediction Research Facility
Monterey, California 93940